arXiv:1403.0819v1 [astro-ph.GA] 4 Mar 2014

Heavy elements in Globular Clusters: the role of AGB stars.

O. Straniero

INAF-Osservatorio Astronomico di Collurania, 64100 Teramo, Italy and INFN-sezione di Napoli, 80126 Napoli, Italy

straniero@oa-teramo.inaf.it

S. Cristallo

INAF-Osservatorio Astronomico di Collurania, 64100 Teramo, Italy and INFN-sezione di Napoli, 80126 Napoli, Italy

L. Piersanti

INAF-Osservatorio Astronomico di Collurania, 64100 Teramo, Italy and INFN-sezione di Napoli, 80126 Napoli, Italy

March 5, 2014

Received _____; accepted _____

ABSTRACT

Recent observations of heavy elements in Globular Clusters reveal intriguing deviations from the standard paradigm of the early galactic nucleosynthesis. If the r-process contamination is a common feature of halo stars, s-process enhancements are found in a few Globular Clusters only. We show that the combined pollution of AGB stars with mass ranging between 3 to 6 $M_{\odot}$ may account for most of the features of the s-process overabundance in M4 and M22. In these stars, the s process is a mixture of two different neutron-capture nucleosynthesis episodes. The first is due to the $^{13}C(\alpha,n)^{16}O$ reaction and takes place during the interpulse periods. The second is due to the $^{22}Ne(\alpha,n)^{25}Mg$ reaction and takes place in the convective zones generated by thermal pulses. The production of the heaviest s elements (from Ba to Pb) requires the first neutron burst, while the second produces large overabundances of light s (Sr, Y, Zr). The first mainly operates in the less-massive AGB stars, while the second dominates in the more-massive. From the heavy-s/light-s ratio, we derive that the pollution phase should last for 150 ± 50 Myr, a period short enough compared to the formation timescale of the Globular Cluster system, but long enough to explain why the s-process pollution is observed in a few cases only. With few exceptions, our theoretical prediction provides a reasonable reproduction of the observed s-process abundances, from Sr to Hf. However, Ce is probably underproduced by our models, while Rb and Pb are overproduced. Possible solutions are discussed.

Subject headings: Stars: AGB — globular clusters: general, chemical composition, multiple populations

1. Introduction

All the elements heavier than iron are mainly produced by neutron captures[1]. There exist two different nucleosynthesis processes of this type, the slow (s) process and the rapid (r) process (Burbidge et al. 1957). Since the typical neutron density of the r process is more than 10 orders of magnitude larger than that of the s process, significantly different physical conditions are implied and, in turn, very different astrophysical environments. The r process is commonly associated with massive stars. Two are the proposed scenarios: core-collapse supernovae (type II, Ib and Ic) and Neutron-Star mergers. Although none of the proposed astrophysical sites has been confirmed by direct observations, the yields of the r process are commonly found in all the Galactic components, very-metal-poor stars included. Such a prompt pollution, demonstrates that the r process takes place in stars that evolves on a very short timescale (see Sneden et al. 2008).

On the contrary, our knowledge of the s-process site has been greatly improved in the last 20 years (for a review see Busso et al. 1999). First of all, it should be reminded that the most abundant products of the s process are the so-called *neutron-magic nuclei*, whose neutron-capture cross section is particularly low compared to the cross section of nearby nuclei. When the s-process flow encounters a neutron-magic nucleus, it acts as a bottleneck, so that its abundance is greatly enhanced with respect to the nearby non-magic nuclei, for which a nearly local equilibrium is established, as given by: $\sigma_A N_A = \sigma_{A-1} N_{A-1}$ [2]. The most important neutron-magic nuclei encountered by the s process are ^{88}Sr, ^{89}Y, ^{90}Zr, ^{138}Ba, ^{139}La, ^{140}Ce, ^{141}Pr, ^{142}Nd, ^{208}Pb and ^{209}Bi. Each of these nuclei corresponds to a peak in

[1]A few isotopes are actually synthesized by the so-called p process whose overall contribution to the elemental abundances is, however, rather small.

[2] $\sigma_A = \frac{<\sigma v>}{v_{th}} = \frac{2}{\sqrt{KT}} \int_0^\infty E\sigma_n(E) exp\left(-\frac{E}{KT}\right) dE$ is the Maxwellian averaged cross section (MACS) and N_A is the fraction of isotopes with atomic mass A.

the distribution of the solar system abundances. The first three are the major contributors to the light-s peak, while those from ^{138}Ba to ^{142}Nd contribute to the heavy-s peak.

As pointed out in the seminal paper of Burbidge et al. (1957), the s process follows simple general rules. Three are the main players: neutrons (or neutron sources), seeds (Fe nuclei) and neutron poisons. The latter are light elements that compete with the seeds in the neutron-capture nucleosynthesis. In this context, a fundamental quantity that characterizes the s process is the neutron-to-seed ratio, i.e., $f = \frac{neutrons-poisons}{seeds}$, where *neutrons, poisons and seeds* represent fractions by number. As firstly shown by Cameron (1957), the synthesis of the heaviest elements, such as Pb, requires a relatively large value of this ratio ($f > 20$), while for low values, namely $f \sim 1$, only light-s are produced. Note that the number of seeds directly scales with the metallicity, so that the production of the heaviest s elements is generally favored at low Z (Busso et al. 1999; Cristallo et al. 2009). As a matter of fact, the cosmic concentration of lead is the result of the pollution caused by low-metallicity AGB stars (e.g., Travaglio et al. 2001). Other important quantities that characterize the s process are the neutron density (N_n), the temperature (T) and the timescale (i.e., the duration of the s-process episode). They determine the time integrated neutron flux, or neutron exposure, namely $\tau = \int N_n v_{th} dt$[3]. Note that the larger the neutron exposure the larger the probability to overshoot the neutron-magic nuclei. Moreover, the Maxwellian averaged cross sections depend on the temperature, while the neutron density is important for the various branchings occurring along the s-process path. Indeed, when a neutron capture produces an unstable nucleus, the β decay may compete with a further neutron capture (see Kappeler et al. 1989). For each branching, it exists a critical value of the neutron density given by the ratio of the decay rate and the neutron-capture rate. When the neutron density is much larger than this critical value, the neutron capture is

[3] v_{th} is the thermal velocity, which depends on T

favored with respect to the β decay, while the opposite occurs at low neutron density. In this way, the neutron density determines the abundances of the isotopes on the alternative paths. Some examples are the branchings at ^{79}Se, ^{85}Kr, ^{95}Zr, ^{134}Cs and ^{151}Sm. In general, those isotopes/elements whose production is sensitive to the neutron density are good estimators of the physical conditions of the s-process site (Lambert et al. 1995; Abia et al. 2001; Aoki et al. 2003; Barzyk et al. 2007; van Raai et al. 2012; Lugaro et al. 2014).

By analyzing the heavy element composition of the solar system, three different components of the s process have been formerly identified, namely the weak, the main and the strong (Seeger et al. 1965; Clayton & Rassbach 1967). Each s-process component implies a specific range of neutron exposures and, in turn, a specific range of the quantities characterizing different s-process sites, i.e., f, N_n, T and the timescale.

The weak component, which includes nuclei with $29 < Z < 40$, is synthesized in the He-burning core and, later on, in the C-burning shell of massive stars (M> 10 $M_\odot$, Raiteri et al. 1991b,a; Kaeppeler et al. 1994; Pignatari et al. 2006). The neutron density may vary from $\sim 10^6$ neutrons/cm^3, in the case of the He burning, up to $\sim 10^{11}$, for the C-burning. Temperatures and timescales are also very different, but the neutron exposure is similar, namely ~ 0.06 mbarn^{-1}. In both cases, neutrons are provided by the ^{22}Ne(α,n)^{25}Mg reaction, so that ^{22}Ne is a necessary ingredient for the weak-s process. In practice, ^{22}Ne is synthesized during He burning, through the ^{14}N$(\alpha,\gamma)^{18}$F$(\beta^+)^{18}$O$(\alpha,\gamma)^{22}$Ne chain, where ^{14}N is that left by the former CNO burning. Therefore, the fraction (by number) of ^{22}Ne nuclei available for the s process in massive stars is approximately equal to the original fraction of C+N+O nuclei. Such an occurrence implies that the synthesis of the weak component is less efficient at low Z, because of the paucity of C+N+O and, in turn, of ^{22}Ne. For instance, during core-He burning, the main neutron poison is ^{25}Mg that is secondary like, since it is directly produced by the ^{22}Ne(α,n)^{25}Mg reaction. As a

result, the weak process yields decrease roughly linearly with metallicity. Instead, in the C-burning shell there are primary like neutron poisons (e.g., ^{16}O, ^{23}Na, ^{24}Mg), which do not depend on the metallicity. Therefore, the s-process efficiency in the C-burning shell is strongly suppressed at low Z (Pignatari & Gallino 2007).

Recently, Pignatari et al. (2008) show that in very low-metallicity fast-rotating massive stars, fresh C synthesized by the 3α reaction may be transported by meridional circulation into the H-rich envelope, thus increasing the amount of C+N+O. They find that this phenomenon would allows an efficient s-process nucleosynthesis, up to Pb. However, in a more recent paper, Frischknecht et al. (2012) argue that this result is due to the use of a particularly low rate of the ^{17}O$(\alpha,\gamma)^{21}$Ne reaction, i.e., that suggested by Descouvemont (1993), which is up to a factor of 1000 lower than the values reported in the widely used reaction rate compilations (Caughlan & Fowler 1988; Angulo et al. 1999). In the He-burning core of fast rotating massive stars, this reaction is expected to destroy most of the ^{17}O released by the poisoning reaction ^{16}O(n,γ)^{17}O. The suppression of the ^{17}O$(\alpha,\gamma)^{21}$Ne favors the competitive channel ^{17}O(α,n)^{20}Ne, so that the neutrons subtracted by the ^{16}O would be recycled. However, new experiments reinvestigated both channels of the ^{17}O+α, confirming previous findings (Best et al. 2011, 2013). In particular, they find that the γ channel is strong enough to compete with the neutron channel, thus leading to a less efficient neutron recycling. Fast-rotating massive stars might still play a role in the production of the weak component (up to Sr), but no significant s-process contribution to heavier elements are expected (see Figure 14 in Best et al. 2013).

The main and the strong components, which include nuclei with $37 < Z < 84$, are produced by low-mass stars ($1.5 < M/M_{\odot} < 2.5$) (Straniero et al. 1995; Gallino et al. 1998; Cristallo et al. 2009, 2011). In these stars, recursive thermonuclear runaways of the shell-He burning, called thermal pulses (TPs), take place during the AGB phase. Two important

events are connected to the occurrence of these thermal pulses. First of all, owing to the excess of nuclear energy released by the thermonuclear runaway, an extended convective instability takes place within the He-rich layer. Later on, owing to the expansion powered by He burning, the shell-H burning dies down and the inner border of the convective envelope can attain the He-rich zone (third dredge up - TDU). The s-process nucleosynthesis in low-mass stars mostly occurs during the relatively long interpulse period ($\sim 10^5$ yr), namely the time elapsed between two subsequent thermal pulses, in a thin radiative layer located at the top of the He-rich zone (Straniero et al. 1995). This layer is known as the ^{13}C pocket, because it is enriched in ^{13}C. The neutron source is the ^{13}C(α,n)^{16}O reaction, which requires a temperature of $\sim 90 - 100$ MK and releases low-density neutron fluxes, i.e., about 10^7 neutrons/cm^3, and neutron exposures between 0.1 and 0.4 mbarn^{-1} (Gallino et al. 1998). A second neutron burst giving rise to a higher neutron density ($> 10^{11}$ neutrons/cm^3) is due to the marginal activation of the ^{22}Ne(α,n)^{25}Mg reaction within the convective zone generated by a thermal pulse, where the temperature may exceed 300 MK. In this case, the timescale is rather short (~ 1 yr), so that the resulting neutron exposure is lower than that of the first neutron burst. These low-mass stars are the main contributors to the s-process elements in the solar system. However, because of their long lifetime (≥ 1 Gyr), it appears that they cannot have contaminated the gas from which the galactic halo formed.

This is the standard paradigm for the heavy element composition of the halo. In practice, only r-process yields are expected in fossil records of the early Galaxy, the s process being hampered by the secondary nature of the neutron sources in massive stars (weak component) and by the too long lifetime of low-mass AGBs (main and strong components). Spectroscopic studies generally confirm such a scenario: single halo stars are r-process enriched, but s-process poor (see Sneden et al. 2008, and references therein). Exceptions are the CEMP-s (Carbon-Enhanced-Metal-Poor stars, where the "s" stay for s-rich). In this case however, the s and the C enrichments are a consequence of mass transfer or wind

accretion in binary systems, a process occurring on a longer timescale (see Bisterzo et al. 2012; Lugaro et al. 2012, and references therein).

In this context, recent spectroscopic studies of Globular Clusters (GCs) revealed a rather different scenario. While the r-process yields generally appear similar to those observed in halo field stars, some GCs show a clear signature of the s-process main component pollution. The few GC stellar populations where an s-process enrichment has been discovered are: M4 (Yong et al. 2008; D'Orazi et al. 2013a), ω-Cen, only stars with [Fe/H]>-1.6 (Smith et al. 2000; Johnson & Pilachowski 2010; D'Orazi et al. 2011), and the redder main sequences of M22 (Roederer et al. 2011) and NGC1851 (Gratton et al. 2012b). Recently, s-process overabundances have been also found in M2 stars (Lardo et al. 2013). Other clusters, like M5 (Ivans et al. 2001; Yong et al. 2008), as well as the most metal-poor stellar populations of ω-*Cen*, M22 and NGC1851, present a "normal" halo distribution of the heavy elements characterized by a pure r-process pollution. These challenging observations represent a further evidence of the existence of multiple stellar populations in GCs. Nevertheless, at variance with other spectroscopic anomalies, such as the O-Na anticorrelation (Gratton et al. 2012a, and references therein), the s-process enhancement is not a common feature of the majority of the GCs in the Milky Way. Therefore, a different class of polluters should be responsible for the heavy-element anomalies. Such a conclusion is also supported by the fact that in M22 and NGC1851 the O-Na anticorrelation is observed in both s-rich and s-poor stars of the same cluster. Moreover, all stars in M4 show a similar overabundance of the s elements but this enrichment is uncorrelated with the [Na/Fe]. More intriguing, some spectroscopic indexes, which depend on the metallicity of the polluters, do not match the theoretical expectations for low-mass AGB stars, which are considered the most important producers of the galactic s-process main and strong components. In particular, the ratio between heavy-s (Ba, La or Nd) and light-s elements (Sr, Y or Zr) are found in solar proportions ([hs/ls]$\sim$ 0]), while an excess of heavy-s is

expected at low Z. Therefore, the polluters responsible for such a peculiar chemical pattern cannot be the same stars responsible for the bulk of the s-process yields in the Galaxy.

In this paper we study the characteristics of the s-process nucleosynthesis in metal-poor AGB stars of low and intermediate mass. We will discuss, in particular, the variations of the nucleosynthesis outcomes with the stellar mass. In the next section we review the most important inputs physics and how they are included in our stellar evolution code. In section 3 we analyse the operation of the two neutron sources active in thermally pulsing AGB stars. This analysis is based on the models presented in section 4. The theoretical yields we derive from these models may be used to test various scenarios for GC formation that have been proposed to explain photometric and spectroscopic evidences of multiple populations, among which: multiple photometric sequences, star-to-star variations of the chemical composition, which cannot be ascribed to internal physical processes, and anomalous color dispersion of horizontal branch stars or the so-called second parameter problem (for a recent review see Gratton et al. 2012a). Several hypotheses about the GC formation have been proposed to explain the new observational framework, such as: inhomogeneities of the primordial material, merging of smaller stellar systems, pollution with external material felt into the gravitational potential well of the cluster and various self-pollution scenarios. Which of these scenarios can also provide an explanation for the s-process enhancements observed in a few GC stellar populations? Which stars are responsible for the s-process contamination in GCs? What are the special conditions determining the onset of this peculiarity? These issues are addressed in section 5 and 6. We show, in particular, that AGB stars with mass ranging between 3 to 6 $M_{\odot}$ can produce the yields necessary to reproduce the observed heavy-element anomalies. In this case, we find that the time elapsed between the formation of the polluters and that of the polluted stellar populations should be of the order of 100-200 Myr.

2. The stellar evolutionary code

All the stellar models presented in this paper have been computed by means of our FUNS code (FUll Network Stellar evolution code)[4]. As illustrated in Straniero et al. (2006) (see also Cristallo et al. 2009, 2011), it includes a full nuclear network of about 500 isotopes (from ^{1}H to ^{209}Bi) and more than 1000 nuclear reactions, coupled to the standard set of 1d hydrostatic differential equations that describe the physical structure. Rotation has been recently included and the resulting effects on the s-process nucleosynthesis occurring in low-mass AGB stars have been discussed in Piersanti et al. (2013). The models here presented are for non-rotating stars. Rotating models for intermediate mass AGB stars will be presented in a forthcoming paper.

The occurrence of recursive thermonuclear runaways makes the computation of AGB evolutionary sequences and the related nucleosynthesis a challenging task for stellar modelers. Numerical algorithms and input physics should be particularly accurate to properly follow significant variations of the physical and chemical structure on relatively small temporal and spatial steps. Many efforts have been made to improve the physical description of these stars and a qualitative agreement is generally found between models produced by different groups, although quantitative results may be rather different. In this section we review the physical processes expected to produce major uncertainties on AGB calculations and how they are treated in the FUNS code.

[4]Such a code has been derived from the FRANEC code (Chieffi & Straniero 1989; Chieffi et al. 1998).

2.1. Mass loss

The AGB mass-loss rates are usually estimated from infrared colors or CO rotational lines. Thanks to the recent progress of the infrared astronomy, our knowledge of the AGB mass loss has been significantly improved (see, e.g., Groenewegen et al. 2009, and references therein). Nonetheless, a general prescription to be used in stellar model calculations is far from being definitely established.

AGB stars are long period variables, Miras or irregulars. In this context, the mass-loss rate versus period relation is an appealing tool for the purpose of stellar model calculations (Vassiliadis & Wood 1993; Whitelock et al. 1994; Schöier & Olofsson 2001; Whitelock et al. 2003; Winters et al. 2003; Groenewegen et al. 2009). Vassiliadis & Wood (1993) firstly use a mass-loss rate versus period relation to calculate AGB models of different masses. In Straniero et al. (2006), we update this relation by means of a more extended set of infrared data. In general, these measurements show that the mass-loss rate remains quite moderate, namely $10^{-8} < dM/dt < 10^{-7}$, for $\log P(days) < 2.5$. For larger periods the mass-loss rate steeply increases and attains maximum values for $\log P > 3$. This upper limit (a few 10^{-5} $M_\odot$/yr) coincides with the superwind phase, which is dominated by a radiation-pressure driven wind (Vassiliadis & Wood 1993). It should be noted, however, that the observed spread of the mass-loss rate versus period relation is rather large. For a given period, the mass-loss rate may vary up to a factor of 10 (see, e.g., Straniero et al. 2006, Figure 5). Nevertheless, it appears that the mass loss versus period relation is a universal feature of AGB stars, independent of stellar mass and envelope composition. For instance, Whitelock et al. (2003) do not find differences between O-rich and C-rich stars, while Groenewegen et al. (2009) exclude a variation with the metallicity. Therefore, it appears that the same mass-loss rate versus period relations can be applied to AGB models of different mass and initial composition. On the contrary, other mass-loss prescriptions,

such as the empirical formula derived by van Loon et al. (2005) or the semi-empirical relation provided by Bloecker (1995), apply to models within a more restricted range of stellar parameters (i.e., initial mass and composition). It should be remarked that most of the available mass-loss studies are based on stars of the Galactic Disk, Galactic Bulge and Magellanic Clouds. Little is known about AGB mass loss for stars with metallicity as low as that of the Galactic GCs.

The mass-loss rate versus period formula used to compute all the AGB models presented in this paper is that described in Straniero et al. (2006). For the pre-AGB phase a classical Reimers' mass-loss rate ($\eta = 0.4$) is used.

2.2. Super-adiabatic convection

In the external convective layers of red giant stars, convective heat transfer only partially accounts for the whole outgoing energy flux. In this case, the effective temperature gradient is larger than the adiabatic one. This is particularly important for AGB stars, where more than 90% of the mass of the convective envelope undergoes super-adiabatic conditions (see Figure 1). The mixing-length theory (MLT; Böhm-Vitense 1958) is widely used to evaluate the super-adiabatic temperature gradient. Being a phenomenological theory, it implies a number of free parameters, usually reduced to just one called α, i.e., the ratio of the average mixing length to the pressure scale height. Note that there exist different versions of the MLT, so that the physical meaning of α may differ from author to author. In our calculation we adopt the formalism described by Cox & Giuli (1968). An alternative phenomenological approach is that proposed by Canuto & Mazzitelli (1991) (hereinafter CM). They consider the full turbulent energy spectrum and set the convective scale length equal to the geometrical depth from the top of the convective region. Comparisons between MLT and CM models show that the CM formalism cannot be reproduced by the MLT

with any constant value of α (Mazzitelli et al. 1995). In practice, the mixing-length free parameter is usually calibrated by reproducing the solar radius with a standard solar model. However, there are no physical reasons to believe that a unique value of α is suitable for any stellar model. Therefore, it may be possible that α should be varied along an evolutionary sequence. This issue has been investigated by Freytag & Salaris (1999) by means of multidimensional radiation hydrodynamics (RHD) simulations covering the range of effective temperatures, gravities, and compositions typical of MS and RGB stars of Galactic GCs. They found that RGB models computed with the α parameter derived from RHD are slightly cooler than those computed adopting a solar calibrated α, (less than 10%), while the CM models predict too low effective temperature. In practice, RGB models would require an α value larger than that needed to reproduce the solar radius. A direct comparison with measured effective temperatures of RGB stars have been also reported by Ferraro et al. (2006) (see also Chieffi et al. 1995). This study confirms previous findings of Freytag & Salaris (1999). Note that a similar comparison cannot be easily obtained with AGB stars, because of the recursive variations of the effective temperature caused by thermal pulses. Since the convective envelope of an AGB star is more similar to that of a RGB star than to the solar convective envelope, all the models presented in this paper have been computed with the MLT and α calibrated on GC RGB stars, namely $\alpha = 2.1$, as reported in Ferraro et al. (2006).

In low-mass AGB stars, a variation of α affects the efficiency of the TDU (e.g., Cristallo et al. 2009, 2011). In addition, since the effective temperature depends on α, the mass-loss rate is also changed. Both these effects modify the heavy element yields. Nevertheless, the relative abundances of Pb, heavy-s and light-s are marginally affected. In massive AGB, a variation of α also affects the maximum temperature attained at the bottom of the convective envelope and, in turn, the nucleosynthesis in the convective envelope and the stellar luminosity (e.g., Iben & Renzini 1983; Ventura & D'Antona 2005).

2.3. Time dependent convection

Owing to the complex nucleosynthesis taking place within the convective regions of AGB stars, which involve a great number of nuclear species, some nuclear burning timescales may be comparable or smaller than the convective turnover timescale. In that case, the assumption of instantaneous mixing, which is usually adopted in computations of pre-AGB stellar models, is no more valid. In case of stars undergoing hot bottom burning (HBB, see Iben & Renzini 1983), high temperatures are attained in the convective envelope during the interpulse period. As an example, for the model shown in Figure 1, the temperature at the bottom of the convective envelope is about 85 MK, which is large enough for the activation of the CN cycle. Note that the extension of the convective envelope of these giant stars is of a few hundreds $R_\odot$ and the average convective velocity, as derived by means of the MLT, is of a few 10^5 cm/s, so that the convective turnover timescale is of the order of 10^8 s. Then, it can be easily verified that the burning timescales of several isotopes involved in the HBB nucleosynthesis are shorter than the convective turnover timescale. For instance, the ^{12}C burning timescale becomes shorter than 10^8 s for T$>$ 60 MK[5]. Therefore, nuclear reactions are faster than the convective mixing, so that partial mixing takes place. Note that the effects of the HBB are overestimated when instantaneous mixing is assumed, with important consequences on both the nucleosynthesis and the HBB contribution to the luminosity. Concerning the convective zone generated by a thermal pulse, convection is usually faster than the α captures, so that the majority of the nuclear species are efficiently mixed. This is not the case of neutrons and protons. The neutron burning timescale is extremely short, so that the neutrons released by the ^{22}Ne(α,n)^{25}Mg reactions are suddenly captured as if they were in a radiative environment. On the other hand, within a C-rich

[5]The ^{12}C burning timescale is given by $\tau_{12} = \frac{1}{\rho r_{12,1} X_H}$, where $r_{12,1}$ is the rate of the ^{12}C$(p,\gamma)^{13}$N reaction, ρ is the density and X_H is the hydrogen mass fraction.

environment where the temperature is of the order of 200-300 MK, as in the convective zone generated during a TP, the proton mobility is also very limited, mainly because of the $^{12}C(p,\gamma)^{13}N$ reactions. Also in this case deviations from the instantaneous mixing must be properly accounted.

The time dependent mixing scheme we use has been described in Straniero et al. (2006). It has been derived from an algorithm originally proposed by Sparks & Endal (1980). In brief, the degree of mixing is calculated by means of the following relation:

$$X_j = X_j^o + \frac{1}{M_{conv}} \sum\nolimits_k (X_k^o - X_j^o) f_{j,k} \Delta M_k \tag{1}$$

where X_j^o and X_j are the mass fractions in the mesh-point j at time t and $t + \Delta t$, respectively. The summation is extended over the whole convective zone. ΔM_k is the mass of the mesh-point k, while M_{conv} is the total mass of the convective zone. The damping factor $f_{j,k}$ is:

$$f_{j,k} = \frac{\Delta t}{\tau_{j,k}} \tag{2}$$

if $\Delta t < \tau_{j,k}$, or

$$f_{j,k} = 1 \tag{3}$$

if $\Delta t \geq \tau_{j,k}$. Here Δt is the time step and $\tau_{j,k}$ is the mixing turnover time between the mesh-points j and k, namely:

$$\tau_{j,k} = \int_{r(j)}^{r(k)} \frac{dr}{v(r)} = \sum\nolimits_{i=j,k} \frac{\Delta r_i}{v_i} \tag{4}$$

The mixing velocity (v_i) is computed according to the MLT.

2.4. Instability of the convective border, third dredge up and ^{13}C pocket

When the convective envelope penetrates the H-exhausted core, a steep variation of the composition takes place at the convective boundary: the H mass fraction drops

from about 70%, within the fully convective envelope, down to zero, in the underlying radiative core. The composition gradient induces a sharp variation of the radiative opacity and, in turn, an abrupt change of the radiative temperature gradient. In these conditions, the precise location of the convective border, as defined by the neutrality condition $\nabla_{rad} = \nabla_{ad}$[6], becomes highly uncertain. Indeed, even a small perturbation causing mixing across the boundary layer induces an increase of ∇_{rad} in the radiative stable zone so that the convective instability moves toward the interior. This situation is commonly encountered in AGB stellar models when a bare Schwarzschild's criterion is used to fix the convective boundaries. It affects both the second and the third dredge up (Becker & Iben 1979; Castellani et al. 1990; Frost & Lattanzio 1996; Castellani et al. 1998; Mowlavi 1999). However, if the effects of such an instability on the second dredge up are probably marginal (Castellani et al. 1998), this is not the case of the third dredge up. Various attempts have been made to overcome such a problem, but a satisfactory solution is still lacking. For instance, Boothroyd & Sackmann (1988) extend to the AGB a method originally developed by Castellani et al. (1985) to treat a similar instability occurring at the outer edge of the convective core during the core-He burning phase. In practice, they try to extend the convective zone, namely: if after mixing the previously stable mesh points become unstable, a further extension of the convective zone is applied, otherwise mixing is limited to the mesh-points where $\nabla_{rad} \geqslant \nabla_{ad}$. A different approach has been followed by Frost & Lattanzio (1996). In stellar evolution codes based on the implicit Henyey method, the convective boundaries are usually calculated once per time step. Instead, Frost & Lattanzio (1996) recalculate the convective boundaries and the corresponding new abundances after each Henyey iteration. This approach should allow to

[6] $\nabla_{rad} = \left(\frac{\partial \log T}{\partial \log P}\right)_{rad}$ and $\nabla_{ad} = \left(\frac{\partial \log T}{\partial \log P}\right)_{ad}$ are the radiative and the adiabatic temperature gradients, respectively.

take into account the feedback of the physical structure due to the variation of the chemical composition induced by mixing. However, severe numerical instabilities are encountered when this procedure is adopted. To overcome such a problem, Frost and Lattanzio set a maximum number of Henyey iterations after which the integration is stopped, even if the stellar structure equations are not satisfied. Note that both Boothroyd & Sackmann (1988) and Frost & Lattanzio (1996) assume, as usually done, i) instantaneous mixing within the convective zone and no extra-mixing beyond the convective boundaries. Actually, the transition between the fully-radiative and the fully-convective zone most likely occurs over a somewhat extended layer, where only a partial mixing takes place. In general, hydrodynamical models of stellar convection confirm the existence of this transition layer (e.g., Freytag et al. 1996; Canuto 1998, 1999; Young et al. 2003, and reference therein). In particular, Freytag et al. (1996) find that the average convective velocity should drop exponentially below the shallow fully-convective envelope of A-type stars and cool white dwarfs. Unfortunately, a limited number of hydrodynamical investigations have been carried out so far for AGB stars undergoing TDU (see, e.g., Young et al. 2003), so that generalized prescriptions for the extension of the transition layer and the strength of the decline of the average convective velocity are not available yet for AGB computations. Nevertheless, owing to the relevance of this phenomenon, AGB models obtained by assuming an exponential decline at the convective boundaries have been developed by various authors (Herwig et al. 1997; Herwig 2000; Mowlavi 1999; Chieffi et al. 2001; Straniero et al. 2006; Cristallo et al. 2009, 2011). In these models, a smooth and stable variable H profile forms at the inner border of the convective envelope, so that the instability occurring at the third dredge up is removed. In addition, the presence of this H profile left in the zone highly enriched in He and C provides the conditions for the formation of the ^{13}C pocket. Note that such an approach necessarily requires the introduction of a free parameter, i.e., the strength of the exponential decline (hereinafter, the β parameter). For instance, in our computation the

average convective velocity within the convective-radiative transition layer is given by:

$$v = v_0 \exp\left(-\frac{d}{\beta H_P}\right) \tag{5}$$

where d is the distance from the formal convective boundary, v_0 is the average velocity of the last unstable mesh point, H_P is the pressure scale height and β is a free parameter. In principle, each convective boundary would require a different β value. Note, however, that within the fully convective zones we calculate v by means of the MLT. In this case $v \propto (\nabla_{rad} - \nabla_{ad})$, so that $v_0 = 0$ when, as usual, the neutrality condition is fulfilled at the convective boundary. In practice, since we consider the average convective velocity, convective overshoot is neglected in our models[7]. On the other hand, $v_0 \gg 0$ during a dredge up (because $\nabla_{rad} \gg \nabla_{ad}$), so that an extramixing naturally araises. Two are the main consequences of this approach, namely i) a deeper dredge up and ii) the development of a ^{13}C pocket. The total mass of ^{13}C in the pocket depends on both the strength of the exponential decline (β in equation 5) and the adopted mixing scheme. Our tests show that when a diffusive scheme is adopted, as in several extant stellar evolution codes, the resulting ^{13}C mass is too small to allow a sizeable s-process nucleosynthesis for any choice of β (see also Herwig 2000). Instead, in our scheme the degree of mixing between two mesh-points depends linearly on the inverse of their reciprocal distance and on the corresponding turnover timescale (see previous section). By means of this mixing scheme and with a proper choice of β, we are able to obtain sufficiently large ^{13}C pockets to account for the bulk of the s-process enhancements measured in AGB stars of relatively low mass (1.5-2.5 $M_\odot$). The variation of the ^{13}C pocket with β and its calibration have been extensively discussed in Cristallo et al. (2009).

[7]With the term "convective overshoot" we intend a mixing beyond the convective boundary in a layer where $\nabla_{rad} - \nabla_{ad} < 0$ both before and after the mixing (see, classical papers by Bertelli et al. 1985; Maeder & Meynet 1987).

2.5. Radiative opacity and equation of state

The occurrence of recursive dredge-up episodes produces significant changes in the chemical composition of the stellar envelope. In principle, a stellar evolution code should account for this phenomenon. In practice, only variations of the main constituents are usually considered. In particular, extant stellar models are based on radiative opacity tables for fixed composition (i.e., scaled solar) except for H and He. This procedure substantially underestimates the radiative opacity of the cool atmosphere of evolved AGB stars, which are highly enriched in C and N. Besides the local thermodynamic conditions, the concentration of the various molecular species basically depends on the atomic abundances. In this respect, an important quantity is the C/O ratio. Among the various molecular species involving C atoms, CO has the larger dissociation energy, so that for C/O<1 almost all the C atoms participate to the formation of this molecule, while the oxygen atoms in excess are free to form other molecules, such as TiO and H_2O. However, when as a consequence of the TDU C/O becomes larger than 1, carbon-bearing molecules, e.g., C_2, CN, C_2H_2, and C_3, dominate the radiative opacity. In addition, if the bottom of the convective envelope attains temperature that are large enough for the activation of the CN cycle, some of the C dredged up is converted into N. Marigo (2002) made a first step toward a correct description of the abundance changes in the calculation of opacity coefficients by estimating molecular concentrations through dissociation equilibrium calculations. Her main finding is the substantial decrease of the effective temperature of C-star models, which implies a huge increase of the mass-loss rate. More recently, Cristallo et al. (2007) (see also Marigo & Aringer 2009) presented new opacity tables with variable amount of C and N. The effects of the adoption of these new opacity tables are particularly strong at low metallicity for which the C+N enhancement in the envelope may be as large as a factor 1000.

The model presented in this paper have been computed with the following prescriptions for the radiative opacity. For T$\leq 10^4$ K we use tables that allow arbitrary enhancements of both C and N and include both atomic and molecular opacity sources (Cristallo et al. 2007). For larger temperature, we have generated specific opacity tables from the OPAL facility (Iglesias & Rogers 1996). Also in this case arbitrary enhancements of C and N are allowed.

The equation of state (EOS) is another critical ingredient of AGB models. An EOS suitable for the high-density regime of the stellar core should account for electron degeneracy and electrostatic interactions (see Straniero 1988). In addition, relativistic corrections should be considered for density $\sim 10^6$ g/cm^3, as it occurs near the stellar center. Partial degeneracy of the electron component takes place in the transition layer between the CO core and the He-rich intershell. At the opposite, in the cool H-rich envelope, partial ionization of atoms and, more outside, molecular recombination produce sizeable modifications of the relevant thermodynamic quantities, such as pressure, specific heat or adiabatic gradient. After various tests devoted to quantify the different contributions to the EOS and their implications for the models, we have adopted the following prescriptions. For T$< 10^6$ K we use the EOS2005 tables provided by the OPAL collaboration (Rogers et al. 1996). These temperatures are usually attained in a great portion of the H-rich envelope, where partial ionization and molecular recombination of the most important chemical species occur. A double interpolation, on hydrogen mass fractions and Z, is performed to account for the variations of the chemical composition due to nuclear burning and/or mixing. Note that in this way the modifications of the envelope composition due to the TDU are not properly taken into account. Indeed, for a given Z, the relative abundances of elements heavier than He are fixed to the scaled-solar values. Nevertheless, we have verified that at variance with the radiative opacity, the interpolation on the total Z provides a good approximation for the EOS. This method is not adequate for the H-exhausted core,

where the contribution to the EOS of elements heavier than He is more important. For this reason, at temperature larger than 10^6 K we use EOS tables for pure elements, as described in Straniero (1988) and Prada Moroni & Straniero (2002). This EOS implies full ionization, which is a quite good approximation for T$> 10^6$ K[8]. Therefore, additivity laws that apply to specific thermodynamic quantities, such as pressure, volume and all the state functions, are exploited to combine the contributions of the various chemical species. The transition across the T$= 10^6$ K boundary is sufficiently smooth.

3. The two neutron bursts

As recalled in the Introduction, two different neutron sources are active in AGB stars undergoing TPs and TDU. In this section we illustrate, on the base of stellar models computed with the FUNS code, the operation of these neutron sources in low metallicity stars of low and intermediate mass. The discussion will be focused on the parameters affecting the nucleosynthesis.

3.1. The radiative ^{13}C(α,n)^{16}O neutron source at low Z

The TDU is a necessary condition for the formation of the ^{13}C pocket. When the convective envelope penetrates the H-exhausted core, down to a layer where the mass fraction of the ^{12}C produced during the previous thermal pulse is about 20%, and, then, recedes, it leaves a variable H profile (see section 2.4). Later on, when this region contracts

[8]Actually, at T$\sim 10^6$ K, this approximation is very good for hydrogen and helium, almost true for the most abundant metals (C, N and O), while iron ions may hold a few of their inner electrons.

and heats up, the $^{12}C(p,\gamma)^{13}N(\beta^+)^{13}C$ chain starts to produce ^{13}C. Then, a ^{13}C pocket forms in the innermost tail of the variable H profile left by the TDU. More outside, owing to the larger H mass fraction, the CN cycle is completed and ^{14}N, rather than ^{13}C, is produced (see panel a) in Figure 2). The temperature in the zone occupied by the thin ^{13}C pocket, which now contains up to a few 10^{-6} $M_\odot$ of ^{13}C, continues to increase during the interpulse period. Later on, when the temperature attains $\sim$ 90 MK, the neutron-capture nucleosynthesys powered by the $^{13}C(\alpha,n)^{16}O$ reaction begins. Initially, the iron seeds in the pocket are rapidly consumed to produce light-s isotopes, up to the first bottleneck corresponding to the magic nuclei ^{88}Sr, ^{89}Y and ^{90}Zr (see panel b) in Figure 2). Then, since at that time most of the iron has been already consumed within the pocket, these light-s nuclei become the main seeds of the s process. While these nuclei are consumed, those belonging to the second bottleneck, such as ^{138}Ba or ^{139}La, are accumulated (panel c) in Figure 2). When the amount of heavy-s overcomes that of the light-s, the amount of ^{13}C is still large and also ^{138}Ba or ^{139}La become seeds, while ^{208}Pb and ^{209}Bi are accumulated (panel d) in Figure 2). Summarizing, the large excess of ^{13}C with respect to the original iron seeds in the pocket leads to the production of a large amount of lead, the end-point of the s process. This occurrence is a common feature of low-mass AGB models with [Fe/H]< -1. By increasing the metallicity, the Pb produced by the ^{13}C burning decreases, but the heavy-s are overproduced with respect to the light-s (see Busso et al. 1999). Finally, if the number of Fe nuclei in the pocket is comparable to (or larger than) the number of ^{13}C nuclei, the main s-process yields are light-s. Such a condition is attained for $Z \geq Z_\odot$. Note that the mass extension of the ^{13}C pocket decreases as the core mass increases. As a result, the largest pockets are those forming at the beginning of the thermal pulse AGB phase. For this reason, in low-mass AGB stars ($M < 3$ $M_\odot$), the s-process nucleosynthesis is dominated by the few (3 or 4) initial ^{13}C bursts (Cristallo et al. 2009). For the same reason, the ^{13}C pockets are smaller in more massive AGB, so that the s-process contribution of the radiative

^{13}C(α,n)^{16}O neutron-capture nucleosynthesis decreases as the stellar mass increases. In massive AGB stars, additional phenomena affecting the development of the ^{13}C pocket should be considered: the hot third dredge up (HTDU, see Goriely & Siess 2004) and the HBB. In the first case, when the convective envelope penetrates into the H-exhausted core (TDU), it encounters hotter layers. If the core mass is large enough, the temperature may be sufficiently high to activate proton capture reactions. Then, the energy released by the nuclear reactions contrasts the convective instability that is pushed outward. This phenomenon has two effects. First, it rises a barrier that limits the TDU. Second, when the convective envelope recedes, it leaves a steeper H profile compared to that obtained in low-mass stars. Therefore, the resulting ^{13}C pockets are smaller. The HBB takes place during the interpulse period in the more massive AGB and in super-AGB stars[9]. In this case, the convective envelope attains layers where the H-burning nucleosynthesis takes place. Then, fresh fuel stored in the cooler portion of the envelope is continuously brought into the burning zone, so that the H-burning rate increases. As firstly demonstrated by Straniero et al. (2000), this rate determines i) the physical conditions at the He ignition, ii) the power of the consequent thermal pulse and iii) the deepness of the following TDU. In particular, the faster the H burning, the weaker the He flash and, in turn, the shallower the following TDU. In summary, the combined action of HTDU and HBB prevents the formation of sizeable ^{13}C pockets and limits the penetration of the convective instability into the H-exhausted core, so that the s-process nucleosynthesis due to the ^{13}C(α,n)^{16}O neutron burst is suppressed. The upper mass limit depends on the metallicity. At Z= 10^{-4}, we

[9]As usual, *AGB stars* are those stars that enter in the AGB phase just after the He-burning phase, while in *super-AGB stars* the AGB phase follows the C-burning phase. The transition mass between the progenitors of AGB and super-AGB stars, the so-called M_{up}, is rather uncertain and depends on both metallicity and He content (Becker & Iben 1979).

found that the ^{13}C neutron source provides a non-negligible contribution to the s-process nucleosynthesis for M$\leq$ 4 M$_\odot$, while at Z=Z$_\odot$ this limit rises up to $\sim$ 5 M$_\odot$. In any case, the core mass should be lower than about 0.9 M$_\odot$. Let us note that the precise value of the maximum mass (or core mass) for the development of sizeable ^{13}C pockets depends on the adopted mixing scheme (see section 2.3). However, as far as we know, no other authors have investigated this limit by means of self-consistent stellar models. Indeed, a proper treatment of both HBB and HTDU requires stellar model calculations performed with a sufficiently extended nuclear network coupled to the stellar structure equations. Only in this case, the calculation may account for all the energetic feedbacks on the physical structure. Nonetheless, the shrinking of the ^{13}C pockets in the more massive AGB is a widely accepted phenomenon (Goriely & Siess 2004). For instance, Lugaro et al. (2012), in their post-process calculations, do not include the nucleosynthesis associated to the ^{13}C pocket in models with M$>$ 4.5 M$_\odot$.

3.2. The convective ^{22}Ne(α,n)^{25}Mg neutron source at low Z

The second neutron burst occurs under very different environmental conditions. First of all, the temperature required to activate the ^{22}Ne(α,n)^{25}Mg reaction is definitely larger, namely about 300 MK. The maximum temperature reached at the bottom of the convective shell generated by a thermal pulse (T_{csh}^{MAX}) depends on the mass of the H-exhausted core (see, e.g., Iben & Renzini 1983): the larger the core mass, the larger T_{csh}^{MAX}. Larger core masses are attained by more massive stars and, for a given mass, by more metal-poor stars. For instance, at Z=0.0001, the ^{22}Ne(α,n)^{25}Mg reaction provides an important contribution to the overall s-process nucleosynthesis for M$>$2.5 M$_\odot$, while at solar metallicity this limit rises up to 3.5 M$_\odot$. At variance with the ^{13}C burning, since the core mass increases as the star climbs the AGB, the ^{22}Ne(α,n)^{25}Mg reaction is more efficient near the AGB tip, when

the temperature within the convective zone generated by the thermal pulse is larger.

Owing to the large temperature (T> 300 MK), the ^{22}Ne burning generates quite large neutron densities, i.e., in between 10^{11} and 10^{13} neutrons/cm^3. As a consequence, some branchings, which are closed in the case of the radiative ^{13}C(α,n)^{16}O neutron burst, are opened, thus allowing alternative s-process paths. Nonetheless, the neutron exposure is not particularly high because of the short duration of a thermal pulse. In addition, the iron reservoir in the convective zone generated by a thermal pulse is large enough to guarantee a sufficiently large amount of seeds for the whole duration of ^{22}Ne burning, even for metallicity as low as Z$\sim$0.0001. Then, the f factor defined in the Introduction does not rich the large values attained in the case of the radiative ^{13}C burning as a consequence of the rapid Fe consumption. For all these reasons, the main yields of the second neutron burst are light-s elements, while heavy-s and Pb are marginally produced.

Note that at variance with massive stars, in AGB stars undergoing TDU the ^{22}Ne(α,n)^{25}Mg reaction may be a primary neutron source. Indeed, the TDU moves primary C from the He-rich intershell to the H-rich envelope. In AGB models with M< 4 M$_\odot$ and low initial metallicity, we find that the C abundance in the envelope attains solar values just after a few TDU episodes. As a result, a relatively high amount of primary ^{22}Ne is piled up within the He-rich layer. In any case, the amount of primary ^{22}Ne in the intershell decreases as the stellar mass increases. Indeed, as already discussed, HBB and HTDU prevent deep TDUs in the more massive AGB models, thus reducing the contamination of the envelope with the ashes of the internal nucleosynthesis. For instance, we find that the s-process contribution is substantially reduced in models with M> 6 M$_\odot$. Such a conclusion confirms previous finding by Doherty et al. (2014). In their super-AGB models most of the neutrons released by the ^{22}Ne(α,n)^{25}Mg reaction are captured by the ^{25}Mg(n,γ)^{26}Mg reaction. As a result, a marginal contribution to the synthesis of heavy elements is expected

from super-AGB stars.

4. The s-process polluters

In this section we present a set of models of AGB stars with mass $2 \leq M/M_{\odot} \leq 6$, [Fe/H]=-1.7, [$\alpha$/Fe]=0.5 and Y=0.245[10]. The corresponding metallicity is Z=7×10^{-4}.

Table 1 reports various properties of these models. In principle, owing to the relatively short lifetime (second column of Table 1), these stars could have time to evolve up to the AGB, thus contaminating the still not-completed building blocks of the early Galaxy. In colum 2 and 3 we report the number of TDU episods and the total mass of the material dredged up, respectively. Note that the average mass dredged up in a single TDU episode decreases as the stellar mass increases. On the contrary, the number of TDU epsidodes increases as the stellar mass increases. As a result the M_{TDU} versus M relation is not linear. In particular, M_{TDU} is practically the same in all models with 3 $\leq$M$\leq$ 5, while in the 6 $M_{\odot}$ model it is the 27% of that of the 2 $M_{\odot}$ model. As it is well known, the maximum peak temperature in the convective shells generated by thermal pulses (column 7) as well as the maximum temperature developed at the base of the convective envelope during the interpulse periods (column 8) increase as the stellar mass (or the core mass) increases (Iben & Renzini 1983). The first temperature affects the efficiency of the convective neutron-capture nucleosynthesis as powered by the ^{22}Ne(α,n)^{25}Mg reaction, while the second temperature determines the efficiency of the HBB. We also report the maximum neutron density corresponding to the maximum peak temperature attained at the base of the convective shells generated by TPs (last column in Table 1). Note that, in spite

[10] The initial composition has been obtained following the procedure described in Piersanti et al. (2007). The reference solar abundance compilation is from Lodders (2003).

of the similar temperature, the maximum neutron densities of the 5.5 and 6 $M_\odot$ models are smaller than that of the 5 $M_\odot$. Such an occurrence is due to the limited dredge up suffered by the more massive AGB stars and, in turn, to the smaller amount of primary ^{22}Ne accumulated in the He-rich intershell (see section 3.2).

In Figure 3 we compare the final surface composition of three of the computed models. In the upper panel we show the 2 $M_\odot$ case. This model represents a typical case of a low-mass AGB stars, characterized by a low core mass, quite deep TDU episodes, low temperature at the base of the convective zone generated by a TP and low temperature at the base of the convective envelope. The nucleosynthesis is dominated by the radiative ^{13}C burning, while the convective ^{22}Ne burning only plays a marginal role and the HBB is negligible [11]. The opposite situation is illustrated in the lowest panel, where the 6 $M_\odot$ case is shown. In this model the ^{13}C pockets are rather small and the corresponding contribution to the s-process nucleosynthesis is marginal. On the contrary, due to the large core mass, the temperature at the base of the convective shell generated by a TP is quite large and the s process powered by the ^{22}Ne(α,n)^{25}Mg reaction is very efficient. These stars also experience a substantial HBB, as clearly shown by the large nitrogen enhancement. The central panel shows an intermediate case, the 4 $M_\odot$ model. In these stars the synthesis of heavy elements is determined by a combination of both the ^{13}C(α,n)^{16}O and the ^{22}Ne(α,n)^{25}Mg neutron bursts. During the first part of the TP AGB phase, the ^{13}C pockets are sufficiently large to power a substantial production of lead and, to a less extent, of heavy-s elements, while

[11]Measurements of C and N in Carbon Enhanced Metal Poor stars (e.g., Johnson et al. 2007) demonstrate that some kind of extra-mixing, deep mixing or cool bottom process should be active in these stars (see also Cristallo et al. 2007). This phenomenon, whose physical origin is a controversial issue, is not included in the models here presented. Note, however, that it does not affect the synthesis of heavy elements.

the lack of ^{22}Ne hampers the second neutron burst. After a few TPs, physical and chemical conditions are reversed. The ^{13}C pockets becomes progressively smaller, while the amount of ^{22}Ne in the He intershell grows up as a consequence of the C dredge up. Then, in the late part of the AGB, the convective ^{22}Ne burning dominates the s-process nucleosynthesis. The synthesis of lead, which is very efficient during the first part of the thermal pulse AGB evolution, reduces significantly after a few TPs, while the production of the light-s elements increases. Note the Rb peak (Z=37) in both the 4 and the 6 $M_{\odot}$ models. This feature is the signature of the high neutron density characterizing the ^{22}Ne neutron burst, which is absent in models with M$\leq$ 2.5 $M_{\odot}$, because of the marginal activation of the second neutron source.

In Table 2 we report the average overabundances in the ejected material of some representative elements, namely:

1) C+N+O. As a consequence of both the first and the second dredge up, material processed by the H burning is mixed into the envelope. As a result, the abundances of C and O decrease, while that of N increases. Nevertheless, the total amount of C+N+O nuclei is conserved. This is not the case of the TDU, which moves into the envelope primary C and, to a less extent, primary O produced by the He burning. As a result, the overabundance of C+N+O at the end of the AGB depends on the efficiency of the TDU and, then, it reflects the variation of M_{TDU} with the initial mass (see Table 1).

2) Fluorine. The AGB production of this element is strictly connected to the ^{13}C(α,n)^{16}O reaction (Lugaro et al. 2004; Abia et al. 2009, and references therein). Indeed, ^{19}F is mainly synthesized by the ^{15}N$(\alpha,\gamma)^{19}$F reaction in the convective zone generated by a TP. ^{15}N may be produced by the ^{18}O$(p,\alpha)^{15}$N reaction, which requires the simultaneous presence of certain amounts of both protons and ^{18}O. This condition is fulfilled in the ^{13}C pocket, where protons are released by the ^{14}N$(n,p)^{14}$C reaction, the main neutron poison,

and ^{18}O mainly by the ^{14}C$(\alpha,\gamma)^{18}$O reaction. If the C+N+O abundance in the envelope is large enough, an additional source of ^{15}N is provided by the ^{13}C left in the H-burning ashes and engulfed in the convective zone generated by a TP. At the beginning of the thermal pulse, this ^{13}C is rapidly consumed by the ^{13}C$(\alpha$,n$)^{16}$O reaction, thus allowing the production of ^{15}N through the same nuclear chain already active in the ^{13}C pocket, with the additional contribution of the ^{14}N$(\alpha,\gamma)^{18}$F$(\beta)^{18}$O reaction. In a low-mass AGB star with solar Z, more than 50% of the fluorine enhancement is due to the ^{13}C left in the H-burning ashes, while at low Z this contribution becomes important in the late part of the AGB, when, as a consequence of the TDU, the C+N+O in the envelope increases. By increasing the stellar mass, the F production decreases, according to the progressive reduction of the ^{13}C pockets mass and of the TDU. In addition, owing to the larger temperature within the convective zone generated by a TP, the two reactions ^{19}F$(\alpha,p)^{22}$Ne and ^{19}F$(n,\gamma)^{20}$F (followed by a β decay into ^{20}Ne) become efficient fluorine destroyers. Finally, in the more massive AGB a further depletion of F is due to the HBB. Since also Pb is a main product of low-mass stars, while it is underproduced in the more massive AGB, a positive correlation between F and Pb is expected in s-rich GC stars.

3) Sodium. Na partecipates to the Ne-Na cycle active in the hottest zone of the H-burning shell. In low-mass AGB stars a further sodium source is provided by the so-called ^{23}Na pocket (Goriely & Mowlavi 2000; Cristallo et al. 2009), as due to an incomplete Ne-Na cycle occurring in the thin layer with variable H profile left by the third dredge up. In addition, neutron captures on ^{22}Ne may produce some ^{23}Na within the He intershell. Therefore, the surface sodium abundance increases after each dredge-up episode. In the more massive AGB, the HBB modifies the surface sodium abundance. It may be produced or destroyed, depending on the maximum attained temperature and on the interplay with the TDU that brings in the envelope additional ^{22}Ne (see Ventura & D'Antona 2006). The large part of the Na enhancement we find in our models with M$>$ 3 M$_\odot$ is a consequence of the second

dredge up, while the HBB and the TDU play a marginal role (see Figure 4). In lower mass models, additional contributions come from the third dredge up. Owing to the combination of different sources, no clear correlations between the Na abundance and the stellar mass can be derived.

4) Y, La and Pb. These three elements are representative of light-s, heavy-s and of the end point of the s-process nucleosynthesis, respectively. Relative abundances are also reported in the last two columns. As expected, lead is the major product of low-mass AGB. Its overabundance decreases as the mass increases. In the more massive models it is underproduced with respect to the light-s. On the contrary, light-s elements are underproduced by low-mass stars, while for M$\geq$ 3.5 M$_\odot$ they are as overabundant as the heavy-s or even more abundant. As for the Pb, the La overabundance decreases as the mass increases.

5) Rubidium. As already recalled, the overabundance of this element with respect to the other light-s, such as Sr, depends on the neutron density developed in the convective ^{22}Ne(α,n)^{25}Mg neutron burst. The nuclei chart in the Rb region is shown in Figure 5. In the radiative ^{13}C(α,n)^{16}O neutron-capture nucleosynthesis, the two major branchings at ^{85}Kr and ^{86}Rb are practically closed, so that the s-process path proceeds through the sequence ^{84}Kr-^{85}Kr-^{85}Rb-^{86}Rb-^{86}Sr and, then, to the neutron magic ^{88}Sr. As a result, the [Rb/Sr]$<$ 0. The case of the ^{22}Ne(α,n)^{25}Mg neutron burst is substantially different. About 50% of the neutron captures on ^{84}Kr directly produce ground state ^{85}Kr, whose β^- decay half-life is 10.756 yr. The remaining 50% feeds the isomeric state of ^{85}Kr (half-life 4.480 h), which decays β^- (78.6%) and γ (21.4%). As a result, about 60% of the neutrons captured by ^{84}Kr produce ^{85}Kr$_g$. Since the temperature at the base of the convective zone generated by a thermal pulse remains above 300 MK for no more than 1 yr (the precise value depends on the mass), ^{85}Kr$_g$ practically behaves as a stable nucleus during the whole neutron-capture

nucleosynthesys episode. Nonetheless, it may capture a neutron producing the neutron magic ^{86}Kr. Then, a further neutron capture would finally lead to ^{87}Rb. However, the latter is hampered by the low MACS of ^{86}Kr, namely 3.4 ± 0.3 mbarn[12]. Indeed, we find that as a consequence of this s-process path, ^{86}Kr is accumulated rather than ^{87}Rb (see also van Raai et al. 2012). Nevertheless, the ^{85}Kr$_g$ remained unburnt at the end of the TP will decay into ^{85}Rb, and, later on, it will be dredge up to the envelope. Note that the efficiency of this Rb source depends on the rather uncertain neutron capture cross section on ^{85}Kr$_g$ (see section 6). The 40% of the ^{84}Kr(n,γ) reactions produces ^{85}Kr$_m$ that suddenly decays β into ^{85}Rb and, after a further neutron capture, leads to ^{86}Rb. Due to the large cross section (202 ± 163), the neutron capture on ^{86}Rb competes with the β decay (half-life 18.63 d), so that a certain amount of the neutron magic ^{87}Rb can be produced. Also in this case, the precise evaluation of the efficiency of this Rb source relies on the rather uncertain MACS of the ^{86}Rb(n,γ) reaction. We have performed some tests to distinguish the various contributions to the Rb synthesis. These tests confirm previous finding of van Raai et al. (2012), namely the dominant contribution is from the ^{86}Rb branching.

The heavy element yields (from Fe to Bi) of the 3, 4, 5 and 6 M$_\odot$ models are compared in Figure 6. Below the Ba peak the yields of the various models are very similar (within a factor of 2), except for the 3 M$_\odot$ that shows a smaller overproduction of all the elements usually ascribed to the weak s-process component($Z < 36$). Above the Ba peak, the differences are definitely more pronounced. If the total La mass ejected by the 3 M$_\odot$ is about 5 time larger than that ejected by the 6 M$_\odot$, the Pb ejected mass is about 30 time larger. As already stated, the more massive AGB stars provide a little contribution to the synthesis of the heaviest s elements.

[12] The values of the cross sections here reported are the 30 KeV MACS from the KADONIS database, (Dillman et al. 2010).

As far as we know, our stellar models are the only ones obtained by coupling the stellar structure equations with a full network of chemical evolution equations. Indeed, s-process calculations in AGB stars are usually obtained by means of post-process codes (Gallino et al. 1998; Goriely & Mowlavi 2000; Lugaro et al. 2012). Probably the main difference concerns the inclusion of the ^{13}C pocket that in post-process calculations is decoupled from the evolution of the physical structure. Indeed, in the extant post-process calculations the same ^{13}C pocket is assumed for the whole evolutionary sequence. As shown by Cristallo et al. (2009), this is a rather crude approximation, because of the natural shrinking of the He-rich intershell and, in turn, of the ^{13}C pocket, due to the increase of the pressure gradient caused by the increase of the core mass occurring during the AGB evolution. Comparisons between our nucleosynthesis results for low-mass stars and those obtained by other authors can be found in several papers. Cristallo et al. (2009) find a qualitative agreement with the s-process calculations of Gallino et al. (1998). Note that the latter were based on old stellar models (Straniero et al. 1997), obtained by using an essential nuclear network, Reimers mass loss and neglecting the modifications of the radiative opacity caused by the TDU. More recently, Lugaro et al. (2012) present new post-process calculations based on updated stellar models with Z=0.0001. In spite on the many differences in both stellar models and nucleosynthesis, their results for low-mass stars are in very good agreement with those we have reported in Cristallo et al. (2009), for both light and heavy elements (see table 5 and 6 in Lugaro et al. (2012)). Concerning more massive AGB stars, the models here presented have an initial composition quite different from that of the Lugaro et al. (2012) models. In particular, the iron abundance (the s-process seed) is about 3 times larger in our models. Recently, D'Orazi et al. (2013b) presented two more models of massive AGB stars, 5 and 6 $M_\odot$, obtained with the same stellar evolution code of Lugaro et al. (2012) (see also Karakas 2010), with total metallicity Z=0.002 and $[\alpha/\mathrm{Fe}]= 0.4$. This composition is more similar to that of a model of 6 $M_\odot$ we have recently computed with our FUNS

code for a work in progress on galactic chemical evolution. The initial iron content is the same as in D'Orazi et al., even if we assume [α/Fe]= 0, so that Z= 0.001. Note that D'Orazi et al. present two models computed under different assumptions for the mass-loss rate, namely Vassiliadis & Wood (1993) and Bloecker (1995), respectively. Like us, they use radiative opacity tables that account for the effects of the TDU (see section 2.5). The evolution of the surface abundances of representative s-process elements of our model are shown in Figure 7. This plot can be directly compared with Figure 11 in the D'Orazi et al. paper. In spite of the many differences of the two stellar models, the overall result appear quite similar. In particular, both calculations show a significant enhancement of Rb and, to a less extent, of other light-s elements (Sr, Y and Zr), while heavier elements are marginally produced. Note that D'Orazi et al. neglect the s-process contribution due to the radiative ^{13}C(α,n)^{16}O burning. The low Pb abundance we find confirms that this is a good approximation for the more massive AGB stars. Nevertheless, they use the ^{22}Ne(α,n)^{25}Mg rate reported in the Angulo et al. (1999) compilation, while we use the more recent Jaeger et al. (2001) that is about 50% smaller at the temperatures of the shell-He burning (about 350 MK). Some minor discrepancies in the resulting surface composition probably reflect such a difference. The TP-AGB lifetime we find is intermediate between those obtained by D'Orazi et al. with the two different choices of the mass-loss rate. Indeed, the mass-loss rate we use is intermediate between Vassiliadis & Wood (1993) and Bloecker (1995) (see section 2.1). Consequently, our final heavy element abundances are in between the two obtained by D'Orazi et al. Once the initial composition is properly re-scaled (our model is for [O/Fe]=0), the final C+N+O of our models is also consistent with the differences in the mass-loss rate. It implies a similar TDU efficiency. On the contrary, the HBB is less efficient in our model. Indeed, at variance with D'Orazi et al., in our model, the C dredged up is only partially converted into N, while O, Na, Mg and Al are very marginally affected by the HBB. This discrepancy may be partially attributed

to different input physics, such as the EOS, interpolation on radiative opacity tables, super-adiabatic convection and the like. However, the use of different mixing schemes may be the main origin of this difference. In particular, at variance with D'Orazi et al., who assume instantaneous mixing, we make use of a time-dependent mixing scheme (see section 2.3).

5. Multiple populations and heavy elements in Globular Clusters

A growing amount of observational evidences, among which multiple sequences in color-magnitude diagrams, extremely blue horizontal branches, cyanogen variations and their anticorrelation with CH, O-Na and Mg-Al anticorrelations, support multiple population (MP) scenarios for the formation of GCs (Cottrell & Da Costa 1981; D'Antona et al. 2005; Gratton et al. 2012a, and references therein). Alternative models, such as the accretion on main-sequence low-mass stars of material lost by more massive objects, have been also proposed (Dantona et al. 1983; D'Antona et al. 2002). Our aim is to verify if these models can also account for the observed s-process pollution and under which conditions this chemical anomaly arises. In the rest of the paper we discuss the case of MP models, even if the yields presented in the previous section may be also used to test accretion models.

MPs may be the result of i) multiple star formation episodes within the same cluster or ii) merging of smaller stellar systems containing a single stellar population. In principle, a combination of the two types is also possible. In any case, the pollution responsible for the observed chemical variations may be due to external stellar populations (primordial-pollution) or caused by the same stars of the cluster (self-pollution). In the following, we will assume that the polluters are normal halo stars, i.e., they form from s-poor

gas with low [Fe/H], [α/Fe]$>$ 0 and [r/Fe]$>$ 0[13]. Moreover, we will not distinguish between primordial-pollution or self-pollution scenarios. Hereinafter the term *first generation* refers to the polluters. As these stars evolve, they lose material containing the imprint of the internal nucleosynthesis. Possibly, this gas is mixed with some amount of residual pristine gas and, then, diluted. The total yield of the stars belonging to this first generation with mass between m and $m + \Delta m$ will be:

$$Y_j = \int_m^{m+\Delta m} \varphi(m) y_j(m) dm \tag{6}$$

where $\varphi(m)$ is the mass distribution function (MF) and $y_j(m)$ is the mass of a given chemical species j ejected by a star with mass m. In the case of a power-law mass function, $\varphi(m) = A \times m^{-\alpha}$. Then, keeping constant the value $y_j(m) = y_j(M_i)$ in the interval $M_i - 0.25 < m < M_i + 0.25$[14], the total yield after a time Δt is given by:

$$Y_j = \sum_{M_{min}(\Delta t)}^{M_{max}} y_j(M_i) \int_{M_i-0.25}^{M_i+0.25} \varphi(m) dm. \tag{7}$$

M_{min} and M_{max} represent the minimum and the maximum initial mass of the stars that are expected to contribute to the s-process contamination of the interstellar gas. M_{min} depends on the duration of the pollution phase (Δt): the larger Δt the smaller M_{min}. The initial mass - stellar lifetime relation, which is equivalent to the M_{min}-Δt relation, is shown in Figure 8, where the solid curve represents a polynomial best fit:

$$\Delta t(Myr) = 10.508 \times M_{min}^4 - 199.62 \times M_{min}^3 + 1422.5 \times M_{min}^2 - 4561.5 \times M_{min} + 5720.5 \tag{8}$$

---

[13] Note that [r/Fe]= 0 in our stellar models. This assumption does not affect the physical evolution of a star. Nonetheless, when comparing our nucleosynthesis predictions to the heavy elements composition of GC stars, the r-process contribution should be properly subtracted from the observed abundances.

[14] Our models are spaced by 0.5 $M_\odot$.

In the following, we will assume $M_{max} = 6$ M$_\odot$, i.e., more massive stars do not contribute to the synthesis of s-process elements. As recalled in the Introduction, fast-rotating massive stars might contribute to the weak component, but here we will limit our analysis to the main and the strong components. Morover, this assumption also implies that we neglect possible contributions to the s process from super-AGB stars (see section 3.2). Then, if the total mass returned to the interstellar medium (m$_{agb}$) is mixed to a certain amount of residual pristine gas (m$_p$), the resulting mass fraction (X_j) is:

$$X_j = X_j^{agb}\frac{m_{agb}}{m_{tot}} + X_j^p\frac{m_P}{m_{tot}} = X_j^{agb}d + X_j^p(1-d) \tag{9}$$

where X_j^{agb} and X_j^p are the mass fractions in the AGB ejecta[15] and in the pristine gas, respectively, $m_{tot} = m_{agb} + m_p$ is the resulting total mass and $d = m_{agb}/m_{tot}$ is the *dilution factor*. Therefore, the overabundance with respect to iron will be:

$$\left[\frac{X_j}{Fe}\right] = \log\left(\frac{X_j^{agb}}{Fe}d + \frac{X_j^p}{Fe}(1-d)\right) - \log\left(\frac{X_j}{Fe}\right)_\odot. \tag{10}$$

Since we assume that the prestine gas is s-process free, X_j^p is zero, so that:

$$\left[\frac{X_j}{Fe}\right] = \log\left(\frac{X_j^{agb}}{Fe}d\right) - \log\left(\frac{X_j}{Fe}\right)_\odot. \tag{11}$$

.

Summarizing, the unknown quantities in this simple model are: Δt, the MF of the first stellar generation and the dilution factor (d). Note that all the constants, such as the total mass of the primordial stellar generation, are canceled when relative abundances are considered.

The resulting undiluted ($d = 1$) compositions for different Δt are compared in Figure 9. Here, we have assumed a power-law MF with $\alpha = 2.35$, namely a classical Salpeter mass

[15] $X_j^{agb} = Y_j/m_{agb}$, where Y_j is the yield of equation 7.

function. As noted by Kroupa (2001), this MF is a reasonable choice for M$\geq$ 3 M$_\odot$. The various curves are shifted in order to have the same [La/Fe] of the $\Delta t = 493$ Myr case. As expected, light-s elements ($Z < 40$) increase by decreasing Δt. In fact, a short timescale implies more massive polluters that are dominated by the neutron-capture nucleosynthesis powered by the convective ^{22}Ne(α,n)^{25}Mg reaction. On the contrary, the abundances of Pb and Bi, mainly produced by the radiative ^{13}C(α,n)^{16}O nucleosynthesis, decrease as Δt decreases. In this way, the relative abundances between Pb, heavy-s and light-s elements are potential indicators of the duration of the pollution phase.

Finally, the effects of a variation of the MF are illustrated in Figure 10. All the models shown in this Figure have $\Delta t = 205$ Myr, but different exponent of the power-law MF, namely: $-5 \leq \alpha \leq 5$. Note that positive α values correspond to the most common case of a MF that decreases as the stellar mass increases. On the contrary, negative α values imply a MF that increases as the mass increases; in that case a maximum of the MF could be located above M$_{max}$. A similar MF has been obtained by Yoshii & Saio (1986) (see also Nakamura & Umemura 2002) in case of extremely metal poor environments. We are aware that this peculiar MF is in contrast with many observational evidences as well as theoretical estimations of the GC mass function. The models here reported should be considered as a test to check the sensitivity of our results on the adopted MF. The various curves have been shifted to match the [La/Fe] value of the $\alpha = 2.35$ case. Note that small α values favor the production of light-s elements, while the Pb abundance is suppressed. In synthesis, if $\alpha \geq 0$ the differences implied by a change of the MF are rather small. The (extreme) case $\alpha = -5$ mimics a moderate reduction of the Δt.

6. Discussion

In the previous sections we have derived the chemical contamination of pristine gas caused by a first generation of intermediate mass polluters. In particular we have shown how the composition of the gas returned to the interstellar medium is expected to change as a function of the duration of the pollution phase that precedes the formation of the stars presently showing an altered heavy-element composition.

In order to test such a theoretical prediction, we have compared the predicted chemical pattern to the observed s-process composition of M22 and M4 stars. For these two clusters, extended samples of heavy element abundances are available. All the stars of M4 so far analyzed present similar overabundances of the s-elements (Yong et al. 2008), while only a subset of M22 members are s rich (Roederer et al. 2011). This difference is likely the result of a different formation history. Nevertheless, as illustrated in the previous section, our model may be applied to both primordial and self-pollution scenarios. Note that the stellar models here used have been computed for [Fe/H]=-1.7. This is quite similar to the value estimated for the first stellar generation of M22, i.e., [Fe/H]= -1.82 ± 0.02 (Marino et al. 2012), but smaller than [Fe/H]~ -1.2 attributed to M4 (Yong et al. 2008). The original iron abundance mainly affects the contribution to the s process due to the radiative ^{13}C(α,n)^{16}O burning. In particular, a reduction of the Pb production is expected by increasing [Fe/H].

The pure s-process pollution in M22 may be obtained by subtracting the average heavy elements composition of the stars belonging to the bluer sequence, those showing r-process enrichment only, to that of the stars belonging to the redder sequence, those showing both r and s enhancements (see Roederer et al. 2011). First of all, Δt has been estimated by means of 5 spectroscopic indexes, namely: [Pb/Y], [Pb/La], [Pb/Ba], [La/Y] and [Ba/Y]. Note that since La and Y are the elements with the smaller spectroscopic errors the [La/Y]

is, in principle, the best Δt indicator. A weighted average of these five indexes leads to $\Delta t = 144 \pm 49$ Myr. In Figure 11 we compare the measured s-process overabundances with those predicted for $\Delta t = 149$ Myr. As usual, the theoretical predictions have been shifted to match the observed La overabundance. Such a shift mimics a certain dilution of the gas ejected by first generation (see equation 11). As a whole, the agreement between the observed and the theoretical chemical pattern is quite good. Few exceptions deserve a closer examination. The most evident concerns the Pb abundance, which is overestimated by our calculations. Lead is mainly produced by the radiative ^{13}C(α,n)^{16}O burning. One may argue that our models overestimate the extension of the ^{13}C pockets in stars with mass larger than 3 $M_{\odot}$. However, smaller pockets cannot be the solution of this discrepancy, because in this case also the heavy s, from Ba to Hf, would be significantly reduced, thus leading to [hs/ls]$\ll 0$, in contrast with the observations. Nevertheless, as discussed in section 3, a reduction of the predicted Pb yield can be obtained by decreasing the neutrons over seeds excess. It may be obtained in various ways: i) reducing the amount of ^{13}C or ii) increasing the amount of iron seeds or iii) increasing the amount of poisons. In a recent paper (Piersanti et al. 2013) we show that in low-metallicity stars, mixing induced by rotation, i.e., Goldreich-Schubert-Fricke instability and meridional circulation, both operating in the He-rich intershell during the interpulse periods, increases the amount of ^{14}N (the main poison) and iron (the main seed) within the ^{13}C pocket, leaving unaltered the total amount of ^{13}C. The net result is a significant reduction of the Pb (and Bi) yield, while the light-s are marginally enhanced and the heavy-s are practically unaffected. A second discrepancy between our theoretical predictions and the observed compositions concerns Ce. In this case the theoretical expectation is smaller than the observed value. Note that the other elements belonging to the heavy-s group, from Ba to Nd are very well reproduced. Then, uncertainties in the nuclear reaction rates involved in the Ce synthesis cannot be excluded. A check in the KADONIS database (Dillman et al. 2010) discloses

that the neutron capture on ^{140}Ce, the neutron magic isotope of Ce, steeply increases between 5 and 10 KeV, corresponding to temperatures between 50 and 120 MK, while it remains almost constant for larger energies and up to 35 KeV (about 400 MK). This behavior substantially differs from that of nearby magic nuclei, ^{138}Ba and ^{139}La, whose neutron capture rates, in the same range of temperature, smoothly decrease (see Figure 12). Such a peculiarity of ^{140}Ce is likely due to the lack of low-energy resonances for the compound nucleus. As a result, the different temperature dependence of the production channel, $^{139}\mathrm{La}(n,\gamma)^{140}\mathrm{La}(\beta^-)^{140}\mathrm{Ce}$, and the destruction channel, $^{140}\mathrm{Ce}(n,\gamma)^{141}\mathrm{Ce}$, favors the Ce production at low temperature ($T < 100$ MK), as it occurs in the case of the radiative $^{13}\mathrm{C}(\alpha,\mathrm{n})^{16}\mathrm{O}$ burning. On the contrary, a lower Ce overabundance with respect to La is expected at larger temperature, as it occurs in the convective $^{22}\mathrm{Ne}(\alpha,\mathrm{n})^{25}\mathrm{Mg}$ neutron burst. Note that a 15% reduction of the ^{140}Ce neutron capture cross section in the energy range 25-35 KeV would reconcile the observed Ce overabundance with the corresponding theoretical prediction. A similar result could be obtained by increasing the $^{139}\mathrm{La}(n,\gamma)^{140}\mathrm{La}$ cross section. These variations are probably within the experimental uncertainties of these nuclear processes.

Other discrepancies between our predictions and M22 heavy elements composition regard elements whose abundance is not only determined by the AGB s-process nucleosynthesis, but may receive contributions from other processes. For instance, Rh (Z=45) is usually ascribed to the r-process, while Cu (Z=29) and Zn (Z=30) are mainly produced by the weak-s process. We recall that the simplified multiple generation model here adopted does not include the possible heavy element pollution due to first-generation stars with M>6 $M_\odot$.

In spite of the mentioned discrepancies, the comparison between the theoretical predictions and the M22 observed chemical pattern is encouraging. The derived dilution

factor, as defined in equation 11, is $d = 0.66$. It implies that the material cumulatively ejected by first-generation stars with M$\leq$ 6 M$_\odot$ should account for about 2/3 of the gas from which the second generation forms. Finally, note that the derived delay time is smaller than the maximum age spread estimated from the double sub-giant branch observed in M22 (Marino et al. 2012).

We have repeated the same analysis with M4. In this case, owing to the lack of s-poor cluster members, the pure s-process component can be extracted by subtracting the average heavy elements composition of M5 from that of M4. Indeed, M5 have a metallicity very similar to that of M4, but it is s-process poor (Yong et al. 2008). The comparison with the predictions of our models is shown in Figure 13. In this case we report the best fits obtained by assuming a power law MF with $\alpha = 2.35$ and -5. The corresponding dilution factors are $d = 0.45$ and $d = 0.67$, respectively. Note the remarkably small value obtained in the case $\alpha = 2.35$, to be compared with the 0.66 of M22, which might be another evidence of the different formation history of this cluster.

Also in this case the theory overestimates the Pb abundance, even in the most favorable case of an extreme MF, while the overall reproduction of the ls and hs is always within the error bars. This occurrence reinforces the need of a mechanism, such as rotation, able to reduce the neutron-to-seed ratio in the ^{13}C pockets of intermediate-mass AGB stars.

The Rb measurement in M4 is particularly interesting. We recall that the synthesis of this element depends on the two branchings at ^{85}Kr and ^{86}Rb, so that its abundance represents a proof of the neutron densities of the s process (see section 4). In particular, a Rb excess, compared to the other light-s, is expected in the case of the convective ^{22}Ne(α,n)^{25}Mg neutron burst. The measured Rb abundance is comparable to the average light-s abundance. In particular, it is larger than the abundances of Sr and Zr, but smaller than that of Y. The scatter of these light-s abundances is likely representative of the true

observational error. As shown in the upper panel of Figure 2 (see also Table 2), [Rb/ls] ≤ -0.4 is expected in the case of a negligible activation of the ^{22}Ne(α,n)^{25}Mg reaction (further details in Cristallo et al. 2011). Therefore, even if the predicted value is larger than the observed one, the Rb measurements in M4 clearly indicate the operation of the convective ^{22}Ne(α,n)^{25}Mg neutron-capture nnucleosynthesis in the s-process polluters. Nevertheless, the models overestimate the observed Rb abundance. Note that the theoretical prediction relies on rather uncertain nuclear physics inputs affecting the ^{85}Kr and ^{86}Rb branchings (see section 4). In particular, only theoretical evaluations are available for the ^{86}Rb neutron-capture cross section. From the KADONIS database we derive that the MACS at 30 KeV is 202 ± 163 mbarn. A reduction of this cross section to the quoted lower limit would reduce the major Rb production channel in intermediate mass AGB stars. On the other hand, for the ^{85}Kr$_g$ neutron capture cross section, we have used the KADONIS prescriptions, also based on theoretical calculations, namely 55 ± 45 mbarn (at 30 KeV). Recently Raut et al. (2013) presented the first experimental evaluation of this cross section. They obtain a 30 KeV MACS of 83^{+23}_{-38}, which is higher than that provided by KADONIS, although compatible within the quoted errors. Note that the higher the ^{85}Kr$_g$ neutron capture cross section the smaller is the amount of ^{85}Kr$_g$ survived at the end of the TP and, in turn, the smaller is the amount of ^{85}Rb accumulated after its slow β decay and, later on, dredged up. Note that an increase of this cross section has minor effects on the overall ^{87}Rb production, because of the very low neutron-capture cross section on ^{86}Kr (see section 4). Therefore, further experimental investigations, as well as other spectroscopic confirmations of Rb abundance in s-rich GC stars are required to solve this problem.

Although the analysis of light elements cannot be limited to the restricted range of stellar masses here considered, some further considerations may be derived from the present study. Among the light elements fluorine deserves a major attention. Until now, F enhancements have been found in AGB stars only or in stars polluted by an AGB

companion, e.g., CEMPs stars (Jorissen et al. 1992; Schuler et al. 2007; Abia et al. 2010, 2011; Lucatello et al. 2011). As shown in section 4, an anticorrelation between the F production and the stellar mass is expected, so that the larger the Δt the higher the fluorine pollution. Recently, D'Orazi et al. (2013c) derived F abundance for a small sample of stars in M22, namely 3 r-only stars plus 3 r+s stars. Although no significant variations of the [F/Fe] is found, the small difference in the average Fe abundance of the two groups of stars may suggest a moderate F enhancement in the r+s stars with respect to the r-only. However, de Laverny & Recio-Blanco (2013) argue that these measurements are affected by an incorrect identification of continuum fluctuations as HF signature and a wrong correction of the stellar radial velocity. Owing to these uncertainties, further investigations are required before considering fluorine measurements in the more general context of GC MP scenarios.

A further comment concerns the sodium pollution by stars with M$\leq$6 M$_{\odot}$. As we have reported in section 3, these stars release a not negligible Na yield. Such a Na is not produced by the HBB, because in these models the convective envelope never attains the layer where the Ne-Na cycle is active. Instead, the Na enhancements are a consequence of the second and, to a less extent, of the third dredge up. If the duration of the pollution phase is sufficiently large, this contribution should be considered in addition to the Na pollution possibly caused by more massive AGB, super-AGB and/or massive stars. This occurrence would imply a deviation from a straight O-Na anticorrelation, leading to a certain spread of Na in stars with similar O. Similarly, since Mg and Al isotopes participate to the neutron-capture nucleosynthesis, also the Mg-Al anticorrelation may be affected by the pollution of intermediate mass AGB stars. In particular, ^{25}Mg is produced by the ^{22}Ne(α,n)^{25}Mg reaction in the He-rich intershell and both Mg and Al isotopes are produced by neutron capture chains starting from ^{22}Ne and ^{23}Na.

7. Conclusions

In this paper we presented new models of low-metallicity AGB stars with mass in the range 2-6 $M_{\odot}$. The heavy elements yields of these models allow us to reproduce most of the observed features of the s-process main and strong components, as shown by stars of some GC stellar populations. The comparison between the theoretical predictions and the observed overabundance of s elements has been done by adopting a simple MP model for the early GC history. This model implies two main temporal steps, namely:

1) a first stellar generation forms from pristine gas whose heavy element composition is that typical of the bulk of the galactic halo, i.e., r rich, but s poor.

2) after about 150 ± 50 Myr, a second stellar generation forms within a newborn GC from the gas ejected by the stars of the first generation, possibly diluted with some amount of pristine gas.

The first generation may or may not be a member of the cluster where the second generation is observed. In other words, the pollution may be either primordial or internal to the cluster (self pollution).

According to this picture, if the star formation definitely halts in less than ~ 50 Myr, namely before that intermediate-mass stars ($M \leq 6\ M_{\odot}$) have time to evolve up to the AGB phase and pollute the interstellar gas, the GC will be s-process poor. This occurrence explains why s-process enhancements are so rare in GCs. It also implies that the more massive stars, whose lifetime is shorter than 50 Myr, do not substantially contribute to the main and strong components of the s process. On the contrary, these stars should be responsible, fully or partially, for the more common variations of C, N, O, Na, Mg, Al and other light elements. For this reason, a more powerful and complete pollution model may be obtained by coupling the yields here presented to those of more massive stars. On the

other hand, physical phenomena not yet included in the present stellar models, such as rotation, may also improve the theoretical tool.

We are grateful to F. Kappeler and I. Dillman, for they help in interpreting the KADONIS reaction rates, and to D. Yong for providing us the M4 and M5 data in a computer readable form. The present work has been support by the PRIN-INAF 2010 and FIRB-MIUR 2008 (RBFR08549F-002) programs. Extended Tables of the models presented in this paper are available in the FRUITY database (fruity.oa-teramo.inaf.it).

REFERENCES

Abia, C., Busso, M., Gallino, R., et al. 2001, ApJ, 559, 1117

Abia, C., Cunha, K., Cristallo, S., et al. 2011, ApJ, 737, L8

Abia, C., Recio-Blanco, A., de Laverny, P., et al. 2009, ApJ, 694, 971

Abia, C., Cunha, K., Cristallo, S., et al. 2010, ApJ, 715, L94

Angulo, C., Arnould, M., Rayet, M., et al. 1999, Nuclear Physics A, 656, 3

Aoki, W., Ryan, S. G., Iwamoto, N., et al. 2003, ApJ, 592, L67

Barzyk, J. G., Savina, M. R., Davis, A. M., et al. 2007, Meteoritics and Planetary Science, 42, 1103

Becker, S. A., & Iben, Jr., I. 1979, ApJ, 232, 831

Bertelli, G., Bressan, A. G., & Chiosi, C. 1985, A&A, 150, 33

Best, A., Görres, J., Couder, M., et al. 2011, Phys. Rev. C, 83, 052802

Best, A., Beard, M., Görres, J., et al. 2013, Phys. Rev. C, 87, 045805

Bisterzo, S., Gallino, R., Straniero, O., Cristallo, S., & Käppeler, F. 2012, MNRAS, 422, 849

Bloecker, T. 1995, A&A, 297, 727

Böhm-Vitense, E. 1958, ZAp, 46, 108

Boothroyd, A. I., & Sackmann, I.-J. 1988, ApJ, 328, 653

Burbidge, E. M., Burbidge, G. R., Fowler, W. A., & Hoyle, F. 1957, Reviews of Modern Physics, 29, 547

Busso, M., Gallino, R., & Wasserburg, G. J. 1999, ARA&A, 37, 239

Cameron, A. G. W. 1957, PASP, 69, 201

Canuto, V. M. 1998, ApJ, 508, L103

Canuto, V. M. 1999, in Astronomical Society of the Pacific Conference Series, Vol. 173, Stellar Structure: Theory and Test of Connective Energy Transport, ed. A. Gimenez, E. F. Guinan, & B. Montesinos, 133

Canuto, V. M., & Mazzitelli, I. 1991, ApJ, 370, 295

Castellani, V., Chieffi, A., & Straniero, O. 1990, ApJS, 74, 463

Castellani, V., Chieffi, A., Tornambe, A., & Pulone, L. 1985, ApJ, 296, 204

Castellani, V., Marconi, M., & Straniero, O. 1998, A&A, 340, 160

Caughlan, G. R., & Fowler, W. A. 1988, Atomic Data and Nuclear Data Tables, 40, 283

Chieffi, A., Domínguez, I., Limongi, M., & Straniero, O. 2001, ApJ, 554, 1159

Chieffi, A., Limongi, M., & Straniero, O. 1998, ApJ, 502, 737

Chieffi, A., & Straniero, O. 1989, ApJS, 71, 47

Chieffi, A., Straniero, O., & Salaris, M. 1995, ApJ, 445, L39

Clayton, D. D., & Rassbach, M. E. 1967, ApJ, 148, 69

Cottrell, P. L., & Da Costa, G. S. 1981, ApJ, 245, L79

Cox, J. P., & Giuli, R. T. 1968, Principles of Stellar Structure (Gordon and Breach)

Cristallo, S., Straniero, O., Gallino, R., et al. 2009, ApJ, 696, 797

Cristallo, S., Straniero, O., Lederer, M. T., & Aringer, B. 2007, ApJ, 667, 489

Cristallo, S., Piersanti, L., Straniero, O., et al. 2011, ApJS, 197, 17

D'Antona, F., Bellazzini, M., Caloi, V., et al. 2005, ApJ, 631, 868

D'Antona, F., Caloi, V., Montalbán, J., Ventura, P., & Gratton, R. 2002, A&A, 395, 69

Dantona, F., Gratton, R., & Chieffi, A. 1983, Mem. Soc. Astron. Italiana, 54, 173

de Laverny, P., & Recio-Blanco, A. 2013, A&A, 560, A74

Descouvemont, P. 1993, Phys. Rev. C, 48, 2746

Dillman, I., Plag, R., Käppeler, F., et al. 2010, in EFNUDAT Fast Neutrons, ed. F.-J. Hambsch, 190

Doherty, C. L., Gil-Pons, P., Lau, H. H. B., Lattanzio, J. C., & Siess, L. 2014, MNRAS, 437, 195

D'Orazi, V., Campbell, S. W., Lugaro, M., et al. 2013a, MNRAS, 433, 366

D'Orazi, V., Gratton, R. G., Pancino, E., et al. 2011, A&A, 534, A29

D'Orazi, V., Lugaro, M., Campbell, S. W., et al. 2013b, ApJ, 776, 59

D'Orazi, V., Lucatello, S., Lugaro, M., et al. 2013c, ApJ, 763, 22

Ferraro, F. R., Valenti, E., Straniero, O., & Origlia, L. 2006, ApJ, 642, 225

Freytag, B., Ludwig, H.-G., & Steffen, M. 1996, A&A, 313, 497

Freytag, B., & Salaris, M. 1999, ApJ, 513, L49

Frischknecht, U., Hirschi, R., & Thielemann, F.-K. 2012, A&A, 538, L2

Frost, C. A., & Lattanzio, J. C. 1996, ApJ, 473, 383

Gallino, R., Arlandini, C., Busso, M., et al. 1998, ApJ, 497, 388

Goriely, S., & Mowlavi, N. 2000, A&A, 362, 599

Goriely, S., & Siess, L. 2004, A&A, 421, L25

Gratton, R. G., Carretta, E., & Bragaglia, A. 2012a, A&A Rev., 20, 50

Gratton, R. G., Lucatello, S., Carretta, E., et al. 2012b, A&A, 547, C2

Groenewegen, M. A. T., Sloan, G. C., Soszyński, I., & Petersen, E. A. 2009, A&A, 506, 1277

Herwig, F. 2000, A&A, 360, 952

Herwig, F., Bloecker, T., Schoenberner, D., & El Eid, M. 1997, A&A, 324, L81

Iben, Jr., I., & Renzini, A. 1983, ARA&A, 21, 271

Iglesias, C. A., & Rogers, F. J. 1996, ApJ, 464, 943

Ivans, I. I., Kraft, R. P., Sneden, C., et al. 2001, AJ, 122, 1438

Jaeger, M., Kunz, R., Mayer, A., et al. 2001, Physical Review Letters, 87, 202501

Johnson, C. I., & Pilachowski, C. A. 2010, ApJ, 722, 1373

Johnson, J. A., Herwig, F., Beers, T. C., & Christlieb, N. 2007, ApJ, 658, 1203

Jorissen, A., Smith, V. V., & Lambert, D. L. 1992, A&A, 261, 164

Kaeppeler, F., Wiescher, M., Giesen, U., et al. 1994, ApJ, 437, 396

Kappeler, F., Beer, H., & Wisshak, K. 1989, Reports on Progress in Physics, 52, 945

Karakas, A. I. 2010, MNRAS, 403, 1413

Kroupa, P. 2001, MNRAS, 322, 231

Lambert, D. L., Smith, V. V., Busso, M., Gallino, R., & Straniero, O. 1995, ApJ, 450, 302

Lardo, C., Pancino, E., Mucciarelli, A., et al. 2013, MNRAS, 433, 1941

Lodders, K. 2003, ApJ, 591, 1220

Lucatello, S., Masseron, T., Johnson, J. A., Pignatari, M., & Herwig, F. 2011, ApJ, 729, 40

Lugaro, M., Karakas, A. I., Stancliffe, R. J., & Rijs, C. 2012, ApJ, 747, 2

Lugaro, M., Tagliente, G., Karakas, A. I., et al. 2014, ApJ, 780, 95

Lugaro, M., Ugalde, C., Karakas, A. I., et al. 2004, ApJ, 615, 934

Maeder, A., & Meynet, G. 1987, A&A, 182, 243

Marigo, P. 2002, A&A, 387, 507

Marigo, P., & Aringer, B. 2009, A&A, 508, 1539

Marino, A. F., Milone, A. P., Sneden, C., et al. 2012, A&A, 541, A15

Mazzitelli, I., D'Antona, F., & Caloi, V. 1995, A&A, 302, 382

Mowlavi, N. 1999, A&A, 344, 617

Nakamura, F., & Umemura, M. 2002, ApJ, 569, 549

Piersanti, L., Cristallo, S., & Straniero, O. 2013, ApJ, 774, 98

Piersanti, L., Straniero, O., & Cristallo, S. 2007, A&A, 462, 1051

Pignatari, M., & Gallino, R. 2007, Mem. Soc. Astron. Italiana, 78, 543

Pignatari, M., Gallino, R., Baldovin, C., et al. 2006, in International Symposium on Nuclear Astrophysics - Nuclei in the Cosmos

Pignatari, M., Gallino, R., Meynet, G., et al. 2008, ApJ, 687, L95

Prada Moroni, P. G., & Straniero, O. 2002, ApJ, 581, 585

Raiteri, C. M., Busso, M., Picchio, G., & Gallino, R. 1991a, ApJ, 371, 665

Raiteri, C. M., Busso, M., Picchio, G., Gallino, R., & Pulone, L. 1991b, ApJ, 367, 228

Raut, R., Tonchev, A. P., Rusev, G., et al. 2013, Physical Review Letters, 111, 112501

Roederer, I. U., Marino, A. F., & Sneden, C. 2011, ApJ, 742, 37

Rogers, F. J., Swenson, F. J., & Iglesias, C. A. 1996, ApJ, 456, 902

Schöier, F. L., & Olofsson, H. 2001, A&A, 368, 969

Schuler, S. C., Cunha, K., Smith, V. V., et al. 2007, ApJ, 667, L81

Seeger, P. A., Fowler, W. A., & Clayton, D. D. 1965, ApJS, 11, 121

Smith, V. V., Suntzeff, N. B., Cunha, K., et al. 2000, AJ, 119, 1239

Sneden, C., Cowan, J. J., & Gallino, R. 2008, ARA&A, 46, 241

Sparks, W. M., & Endal, A. S. 1980, ApJ, 237, 130

Straniero, O. 1988, A&AS, 76, 157

Straniero, O., Chieffi, A., Limongi, M., et al. 1997, ApJ, 478, 332

Straniero, O., Gallino, R., Busso, M., et al. 1995, ApJ, 440, L85

Straniero, O., Gallino, R., & Cristallo, S. 2006, Nuclear Physics A, 777, 311

Straniero, O., Limongi, M., Chieffi, A., et al. 2000, Mem. Soc. Astron. Italiana, 71, 719

Travaglio, C., Gallino, R., Busso, M., & Gratton, R. 2001, ApJ, 549, 346

van Loon, J. T., Cioni, M.-R. L., Zijlstra, A. A., & Loup, C. 2005, A&A, 438, 273

van Raai, M. A., Lugaro, M., Karakas, A. I., García-Hernández, D. A., & Yong, D. 2012, A&A, 540, A44

Vassiliadis, E., & Wood, P. R. 1993, ApJ, 413, 641

Ventura, P., & D'Antona, F. 2005, A&A, 431, 279

—. 2006, A&A, 457, 995

Whitelock, P., Menzies, J., Feast, M., et al. 1994, MNRAS, 267, 711

Whitelock, P. A., Feast, M. W., van Loon, J. T., & Zijlstra, A. A. 2003, MNRAS, 342, 86

Winters, J. M., Le Bertre, T., Jeong, K. S., Nyman, L.-Å., & Epchtein, N. 2003, A&A, 409, 715

Yong, D., Karakas, A. I., Lambert, D. L., Chieffi, A., & Limongi, M. 2008, ApJ, 689, 1031

Yoshii, Y., & Saio, H. 1986, ApJ, 301, 587

Young, P. A., Knierman, K. A., Rigby, J. R., & Arnett, D. 2003, ApJ, 595, 1114

This manuscript was prepared with the AAS LaTeX macros v5.2.

Table 1. Physical properties of the computed stellar models: initial mass ($M_\odot$), total lifetime (Myr), n. of TPs followed by a TDU, total dredge-up mass (10^{-2} $M_\odot$), final core mass ($M_\odot$), total ejected mass ($M_\odot$), maximum peak temperature attained at the bottom of the convective shells generated by thermal pulses (MK), maximum temperature attained at the bottom of the convective envelope during the AGB (MK), neutron density corresponding to the maximum peak temperature attained at the bottom of the convective shells generated by thermal pulses (10^{13} neutrons/cm^3).

Mass	lifetime	n. TPs	M_{TDU}	M_H^f	ejected mass	T_{csh}^{MAX}	T_{ce}^{MAX}	n_n
2.0	861	10	7.5	0.670	1.330	320	4	< 0.1
2.5	493	13	6.7	0.725	1.775	342	6	0.1
3.0	302	15	3.9	0.814	2.186	347	11	0.5
3.5	205	19	3.9	0.850	2.650	365	19	0.8
4.0	149	23	3.9	0.875	3.125	366	22	0.9
4.5	113	29	3.9	0.909	3.591	367	30	1.1
5.0	90	35	3.5	0.947	4.053	371	43	1.8
5.5	73	48	3.0	0.996	4.504	373	73	1.5
6.0	61	72	2.0	1.052	4.949	371	91	0.8

Table 2. Average composition of the ejected material.

Mass	$\left[\frac{C+N+O}{Fe}\right]$	$\left[\frac{F}{Fe}\right]$	$\left[\frac{Na}{Fe}\right]$	$\left[\frac{Rb}{Fe}\right]$	$\left[\frac{Y}{Fe}\right]$	$\left[\frac{La}{Fe}\right]$	$\left[\frac{Pb}{Fe}\right]$	$\left[\frac{La}{Y}\right]$	$\left[\frac{Pb}{Y}\right]$
2.0	1.69	2.02	0.80	0.53	0.85	1.37	2.69	0.52	1.84
2.5	1.57	1.91	0.75	0.66	0.76	1.24	2.60	0.48	1.84
3.0	1.38	1.57	0.55	0.98	1.00	1.36	2.49	0.36	1.49
3.5	1.32	1.31	0.68	0.98	0.83	1.07	2.20	0.24	1.13
4.0	1.29	1.06	0.80	1.06	0.81	0.87	1.95	0.06	1.13
4.5	1.24	0.76	0.87	1.06	0.76	0.63	1.60	-0.13	0.84
5.0	1.19	0.49	0.91	1.10	0.78	0.48	1.26	-0.30	0.48
5.5	1.14	0.28	0.97	1.07	0.77	0.44	1.00	-0.33	0.23
6.0	0.97	-0.08	0.97	0.81	0.53	0.22	0.37	-0.31	-0.16

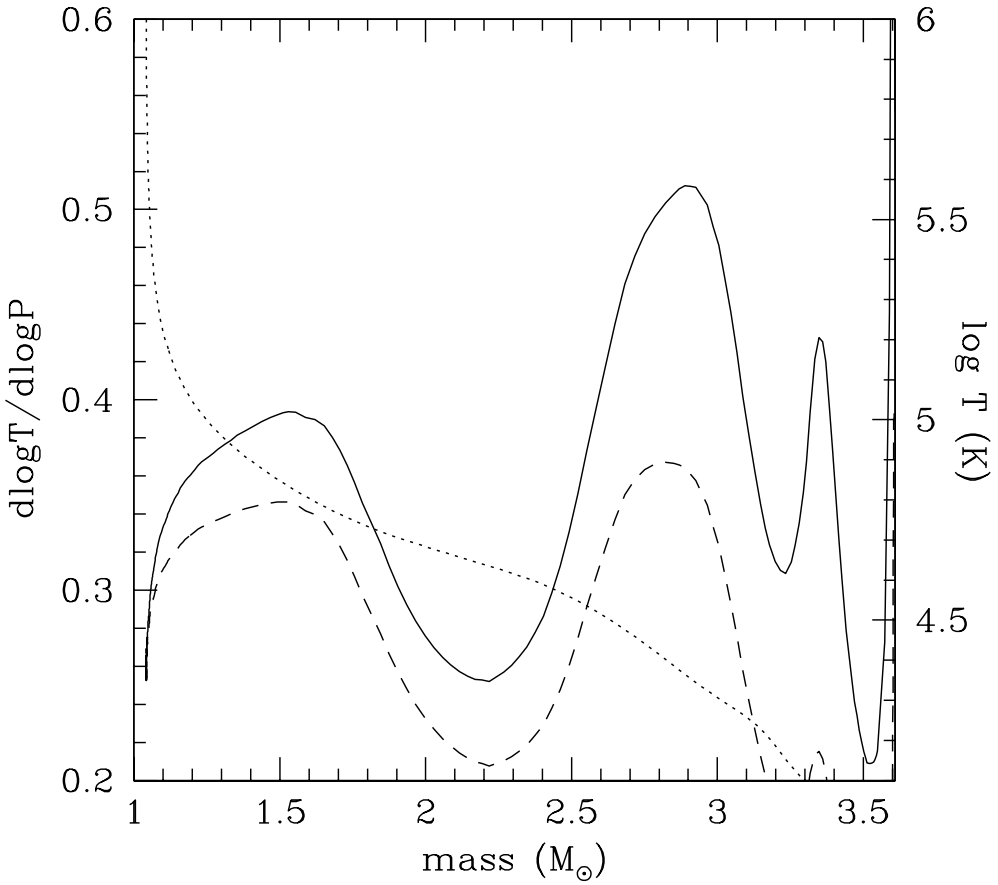

Fig. 1.— Temperature gradients within the convective envelope of a 6 $M_\odot$ model during the 50th interpulse period: effective gradient (solid line), adiabatic gradient (short-dashed line). The temperature profile is also shown (long-dashed line). Note that the temperature at the convective boundaries, i.e., 85 MK (internal) and 4000 K (external), are out of the Y axis range.

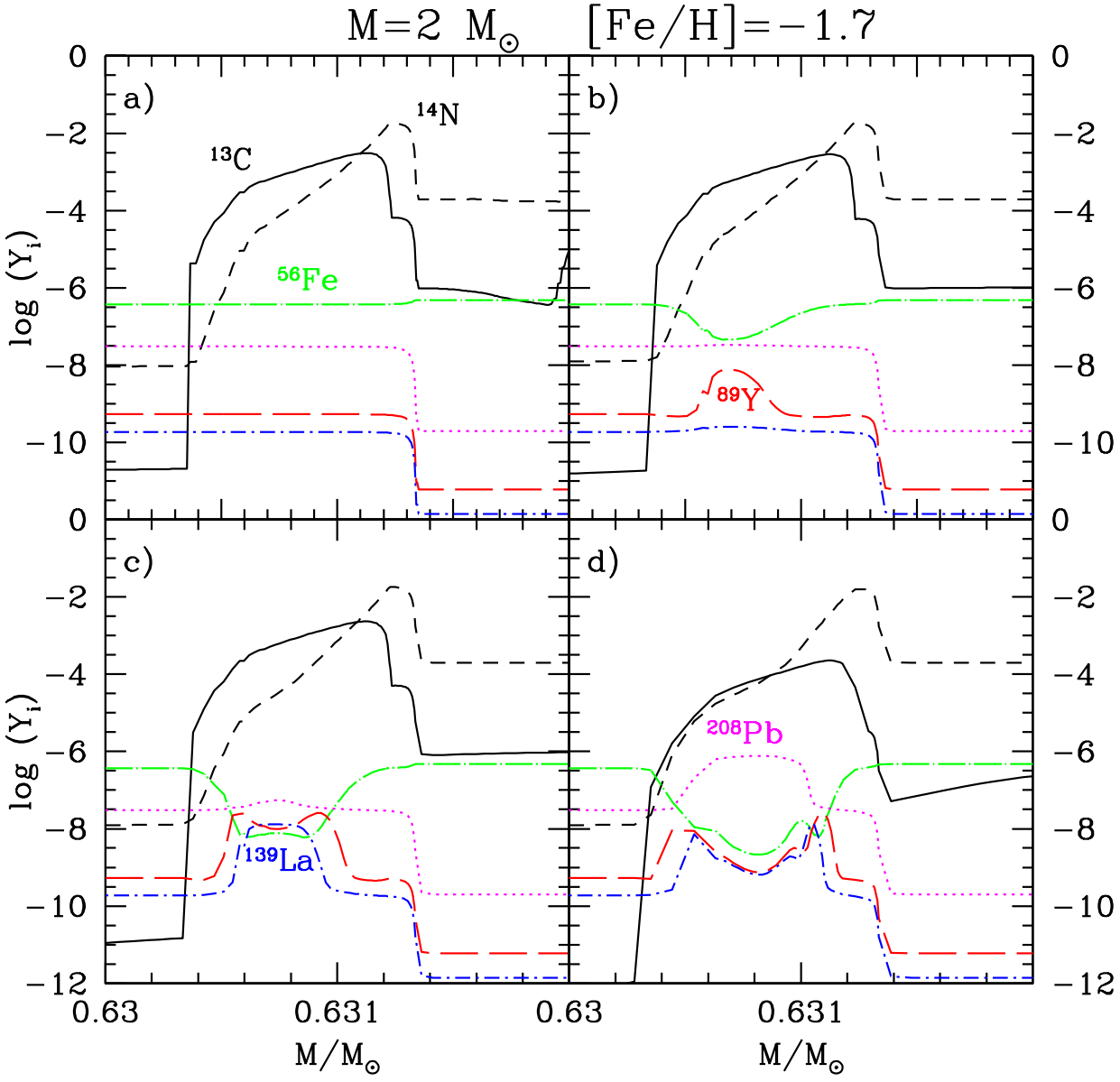

Fig. 2.— Evolution of some chemical species within the third fully developed ^{13}C pocket of the 2 $M_\odot$ model. Panel a): the pocket formation is completed; panel b): the early phase of the radiative s-process nucleosynthesis, characterized by the production of light-s elements; panel c): intermediate phase during which heavy-s elements are mainly produced; panel d) the late part of the s process, when a huge amount of Pb is synthesized into the pocket.

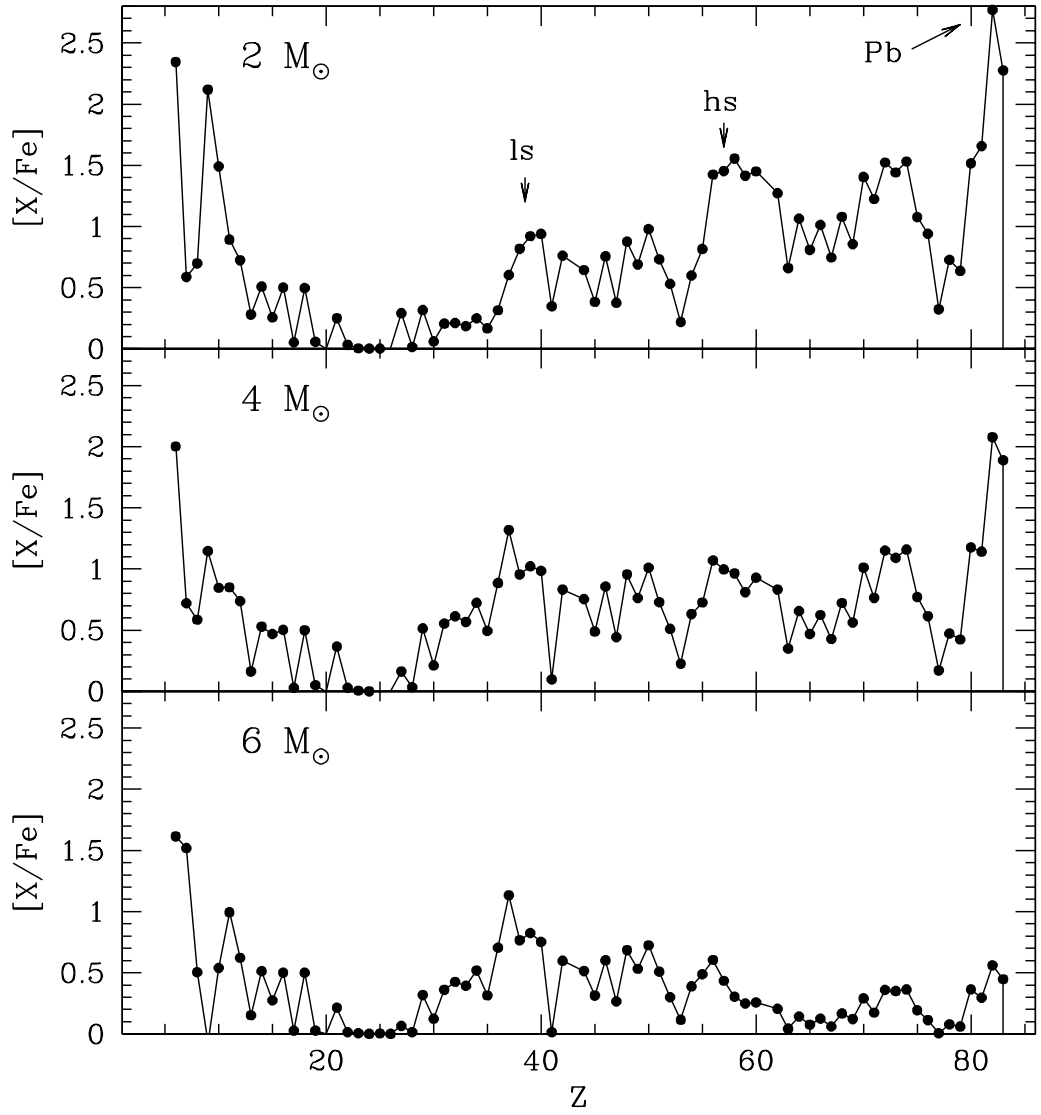

Fig. 3.— Final compositions of the 2, 4 and 6 $M_\odot$ models with [Fe/H]=-1.7, [α/Fe]=0.5 and Y=0.245.

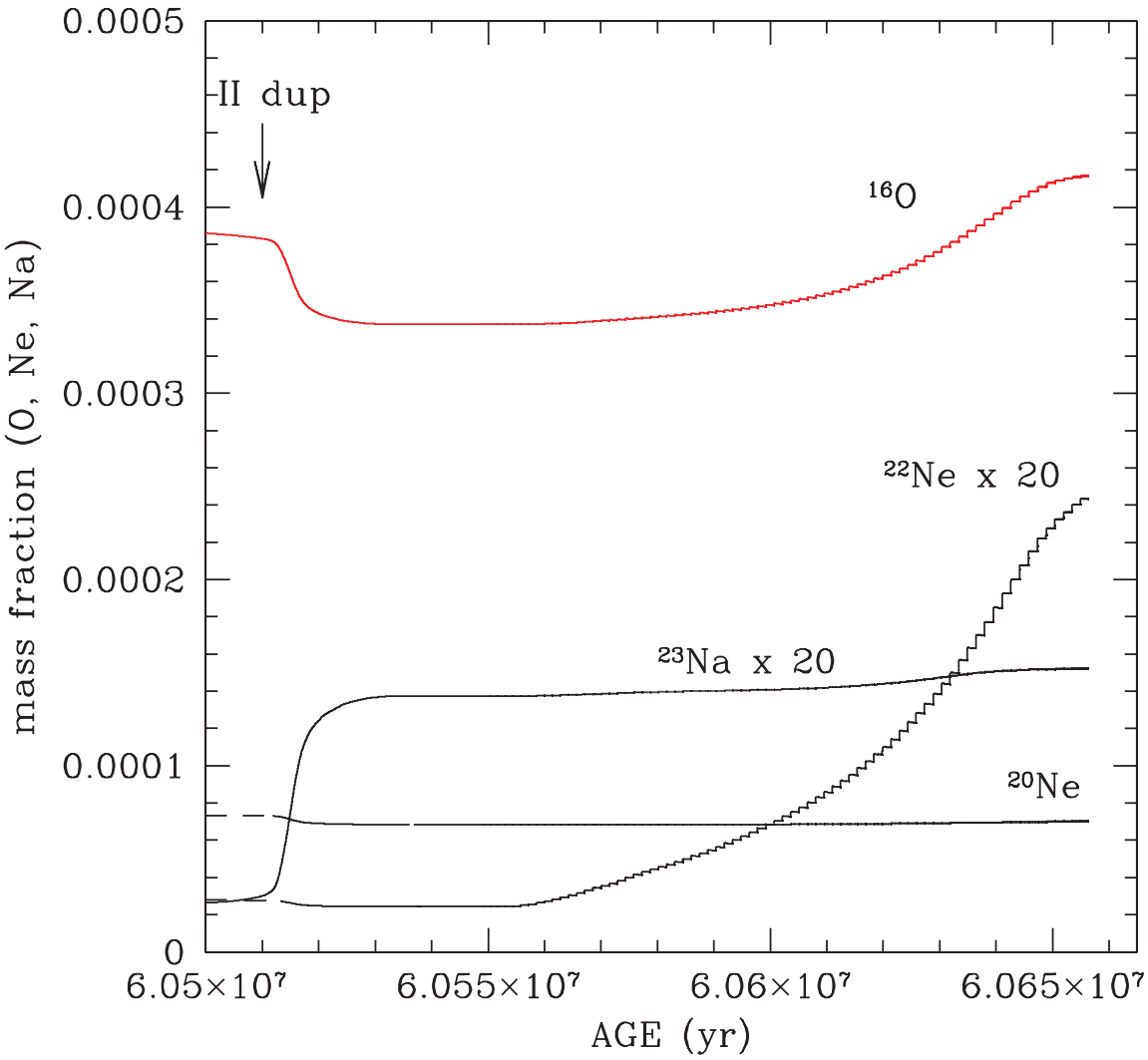

Fig. 4.— Evolution of ^{16}O, ^{20}Ne, ^{22}Ne and ^{23}Na at the surface of the 6 $M_{\odot}$ model. ^{16}O is depleted after the second dredge up and, later on, it is restored to nearly the initial abundance by the TDU, which attain the region enriched with primary O during the preceding TP. The two major Ne isotopes are not affected by the second dredge up. However, ^{22}Ne abundance increases after each TDU. ^{23}Na is enhanced after the second dredge up, while a negligible increase is observed as a consequence of the TDU. Finally, no one of these isotopes are affected by the HBB.

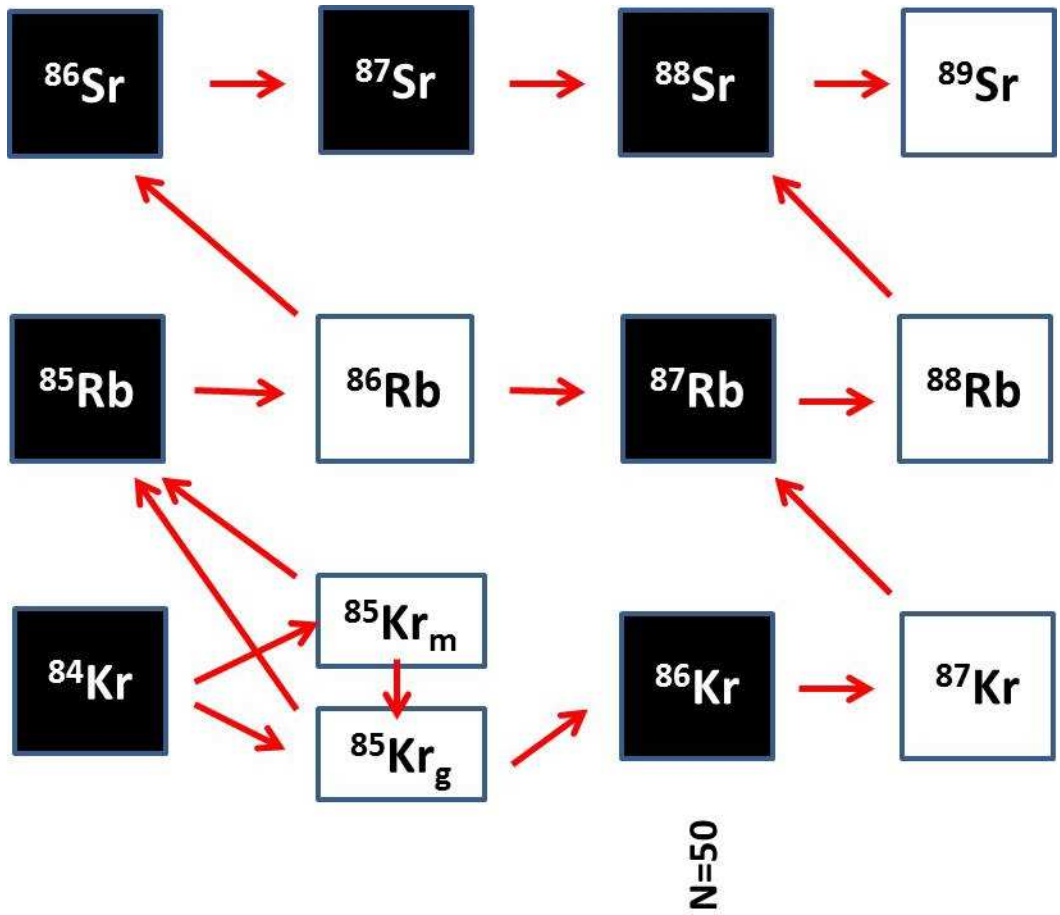

Fig. 5.— The s-process path in the Kr-to-Sr region. Empty squares represent unstable nuclei, while arrows show the alternative s-process paths

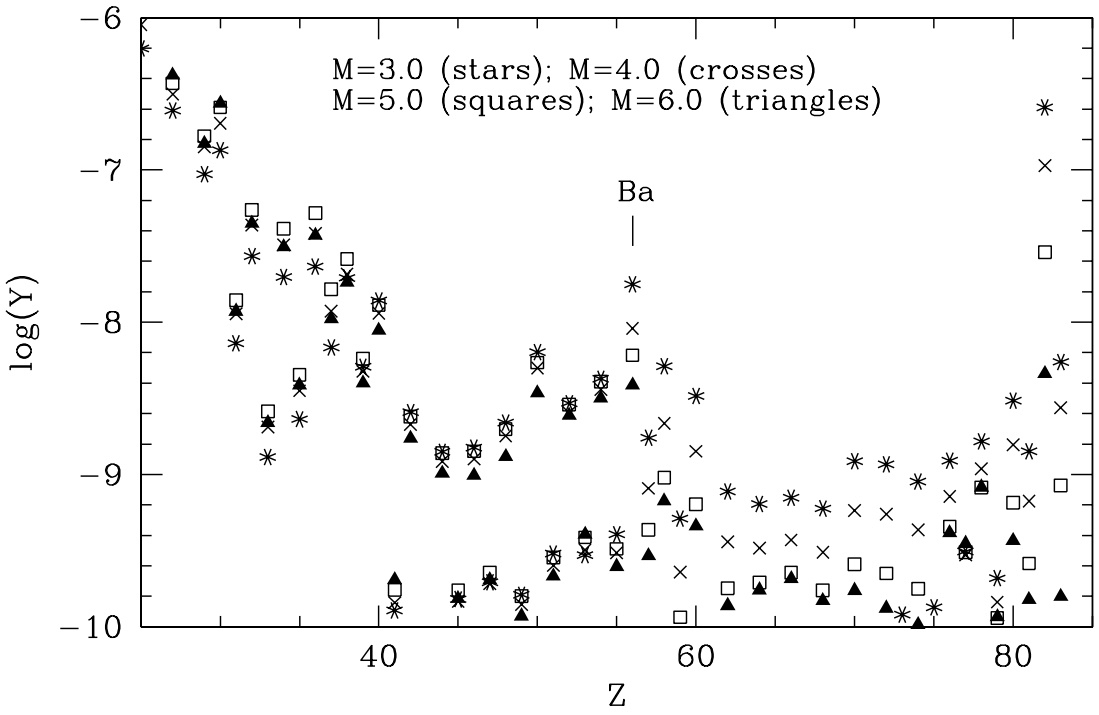

Fig. 6.— Total yields, i.e., the total mass of a given element (in $M_\odot$) in the material ejected by the star during its whole life. Results for models with initial mass 3, 4, 5 and 6 $M_\odot$ are here compared.

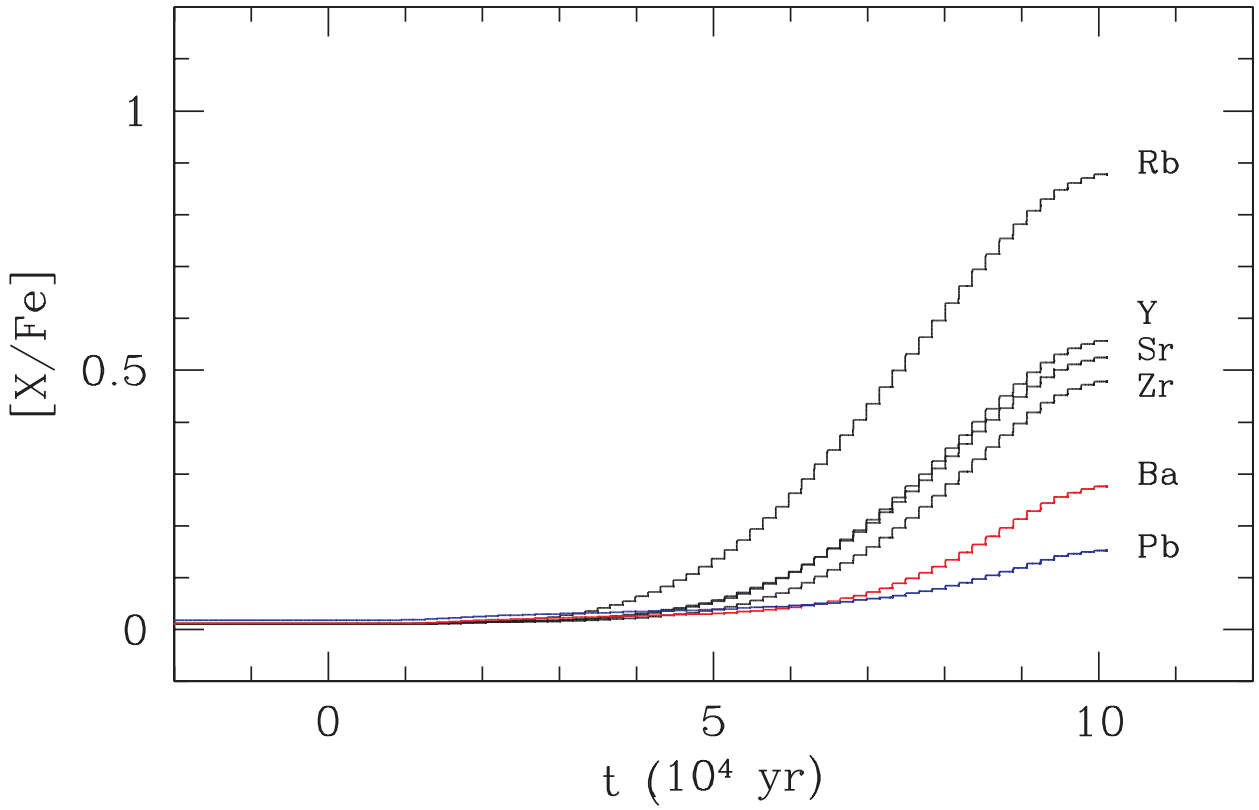

Fig. 7.— Evolution of the s process surface abundances for a model of M=6 $M_{\odot}$ and Z=0.001.

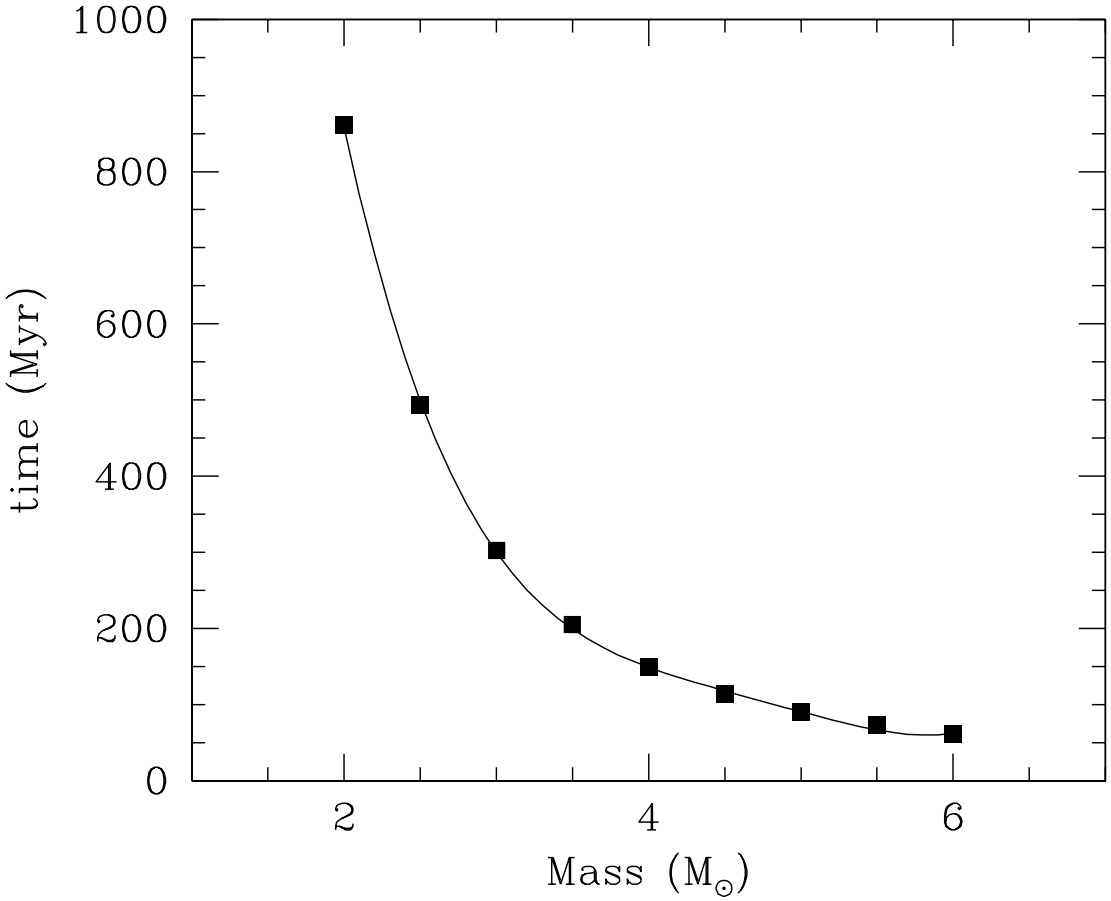

Fig. 8.— Stellar lifetime versus initial mass.

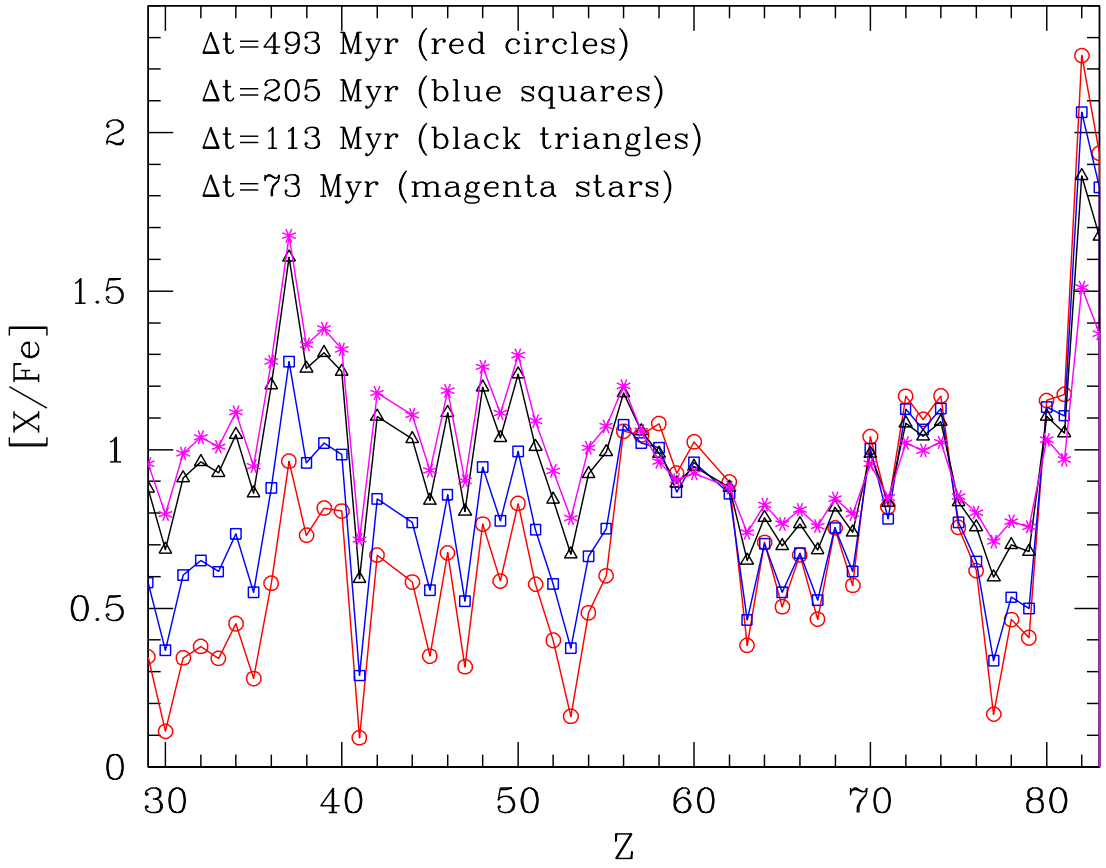

Fig. 9.— Average composition of the material ejected by the first generation AGB stars. The various curves refer to different delay times (see text). They are shifted to the same [La/Fe].

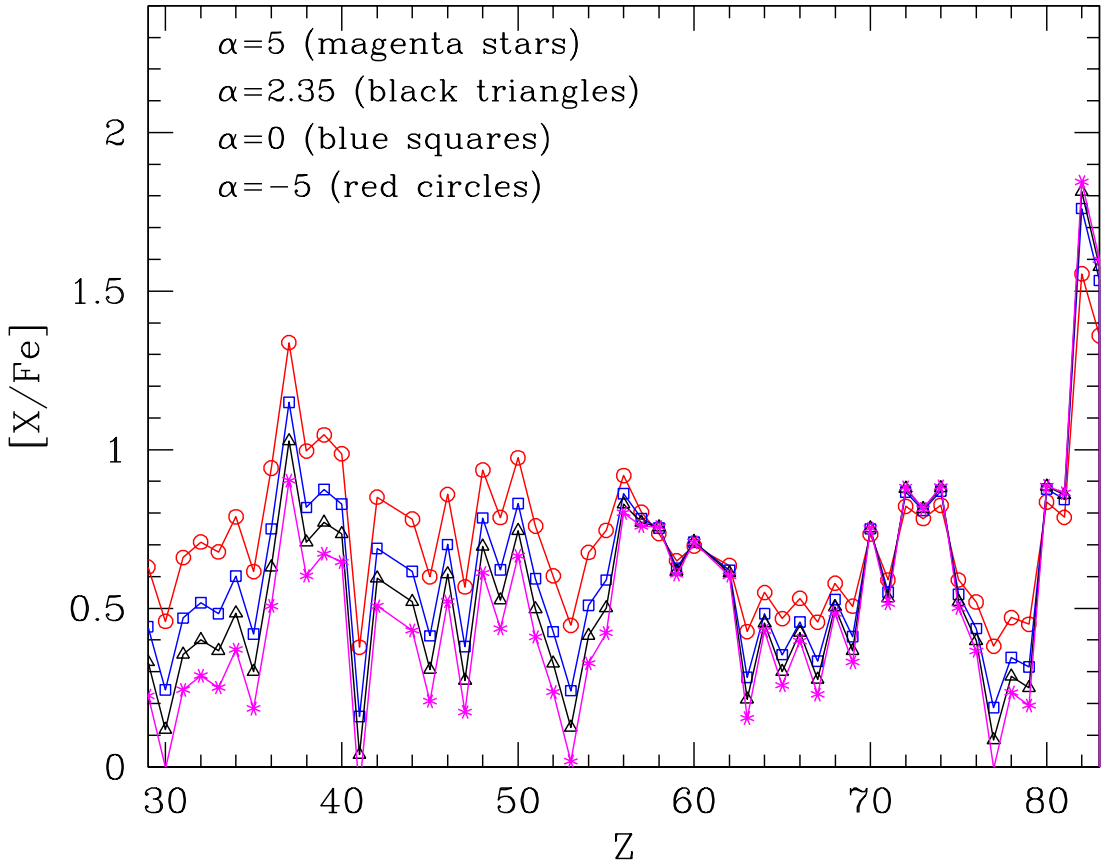

Fig. 10.— Average composition of the material ejected by the first generation AGB stars (Δt = 205 Myr). The various curves have been obtained by varying the exponent of the power-law mass function. As in Figure 9, they are shifted to the same [La/Fe].

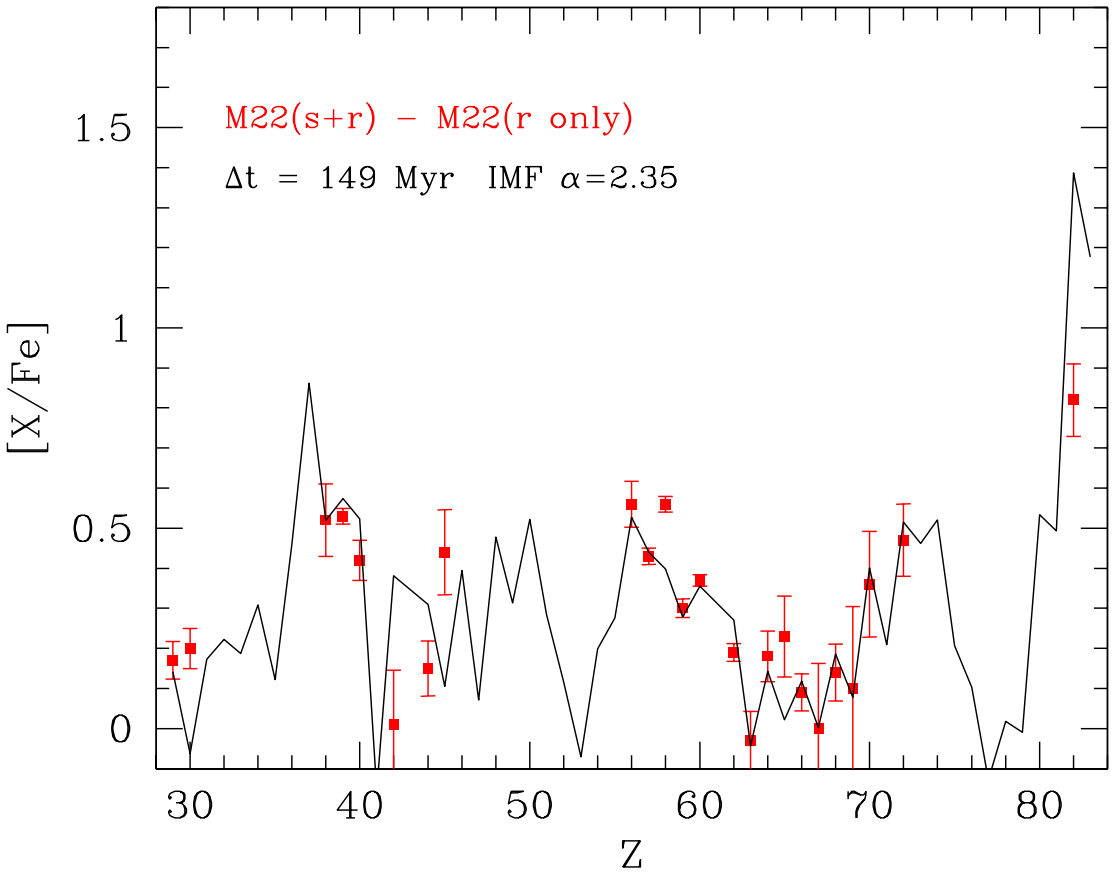

Fig. 11.— Best fit of the average s-process chemical pattern of stars in M22.

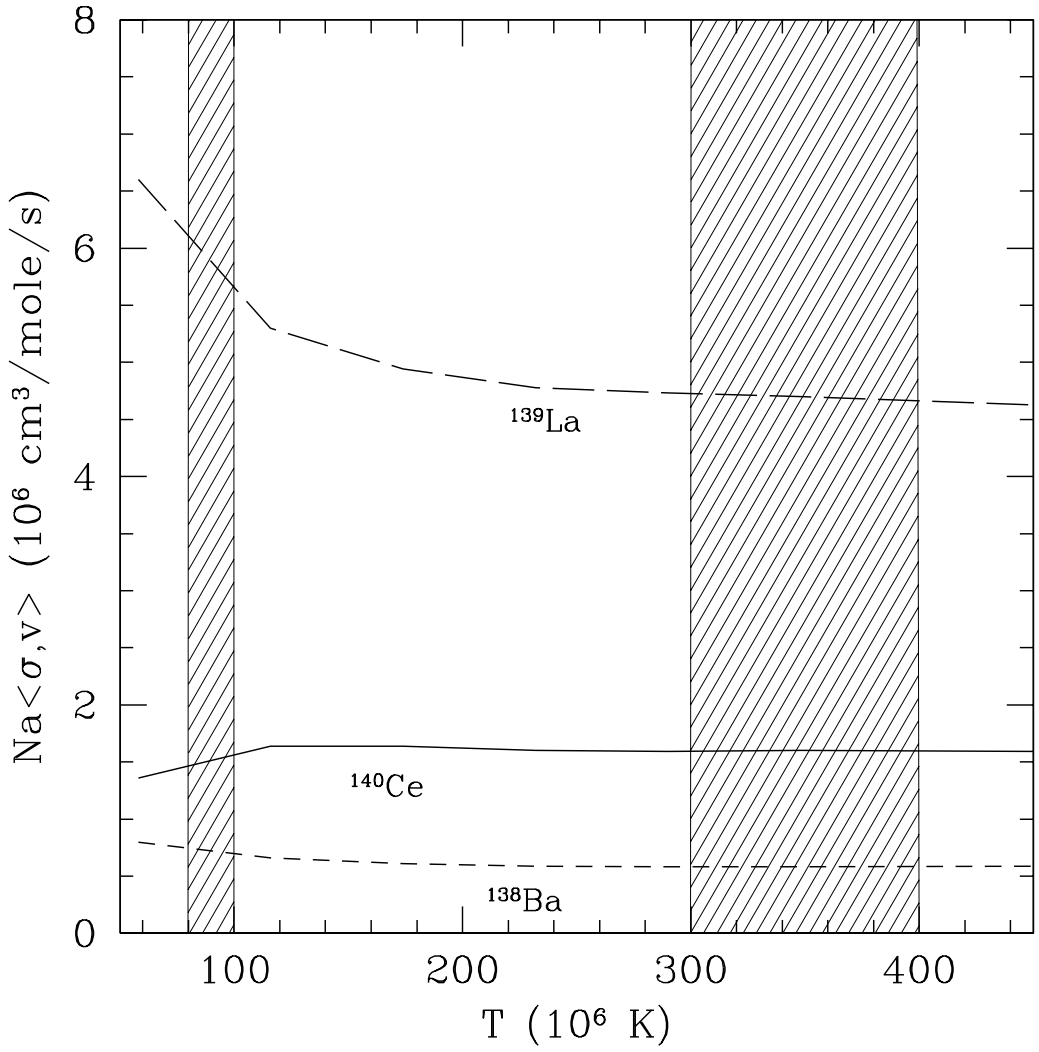

Fig. 12.— Neutron capture reaction rates of some magic nuclei belonging to the heavy-s group as a function of the temperature. The two shaded areas indicate the ranges of temperature experienced during the ^{13}C(α,n)^{16}O and the ^{22}Ne(α,n)^{25}Mg burnings, respectively. Note the diversity of ^{140}Ce with respect to the nearby magic nuclei.

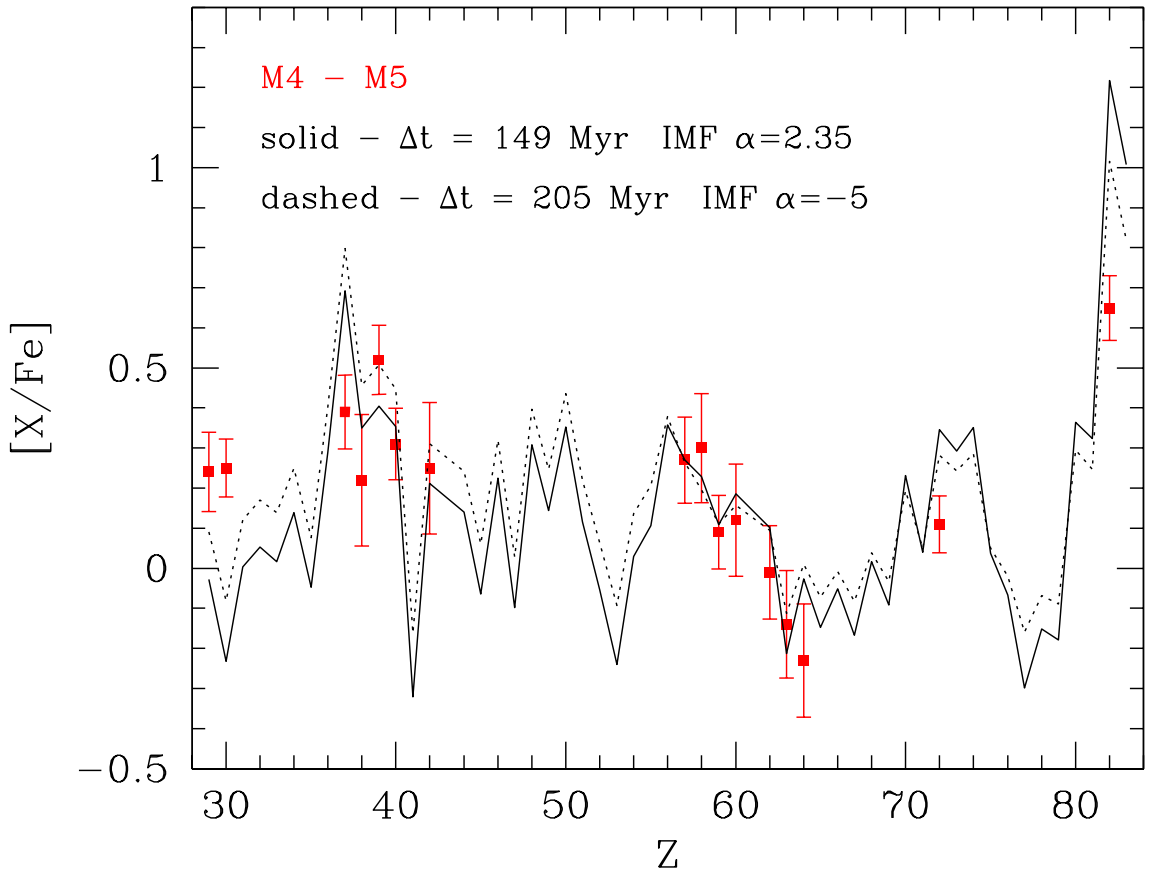

Fig. 13.— Best fit of the average s-process chemical pattern of stars in M4.